



Water Resources Research®

RESEARCH ARTICLE

10.1029/2023WR036056

Key Points:

- Geologic heterogeneity inhibits salt finger formation in beach aquifers and promotes a stable mixing zone due to enhanced dispersion
- Intertidal saltwater-freshwater mixing zones are most stable under high degrees of heterogeneity and high geologic continuity
- Results provide a possible explanation into the lack of field observations of fingering flow in beach aquifers

Supporting Information:

Supporting Information may be found in the online version of this article.

Correspondence to:

J. W. Heiss,
james_heiss@uml.edu

Citation:

Olorunsaye, O., & Heiss, J. W. (2024). Stability of saltwater-freshwater mixing zones in beach aquifers with geologic heterogeneity. *Water Resources Research*, 60, e2023WR036056. <https://doi.org/10.1029/2023WR036056>

Received 10 AUG 2023

Accepted 8 JUN 2024

Stability of Saltwater-Freshwater Mixing Zones in Beach Aquifers With Geologic Heterogeneity

Olasunkanmi Olorunsaye¹ and James W. Heiss¹ 

¹University of Massachusetts Lowell, Lowell, MA, USA

Abstract Saltwater-freshwater mixing zones in beach aquifers support biogeochemical reactions that moderate chemical loads in fresh groundwater discharging to marine ecosystems. Existing laboratory and numerical modeling studies have demonstrated that fluid density gradients in the mixing zone can lead to free convection and the formation of density instabilities, or salt fingers, under a range of hydrologic, morphologic, and hydrogeologic conditions. However, salt fingers have rarely been observed in real-world beach aquifers despite a growing body of field studies investigating intertidal mixing zones. In this study, we used geostatistical methods to generate randomly distributed assemblages of fine and medium sand and incorporated those geologic realizations into variable-density variably-saturated flow and salt transport simulations to explore the influence of geologic structure on mixing zone stability in tidally-influenced beaches. Ensemble-averaged model results show that geologic heterogeneity inhibits salt finger formation and promotes a stable intertidal mixing zone due to enhanced dispersion. This effect is highest for high degrees of heterogeneity and for more laterally connected geologic architecture. Compared to hydraulically equivalent homogeneous models, sediments with moderate to high heterogeneity produce mixing zones that are on average 19%–29% smaller and 3–10 times more stable due to the absence of the downward convection and seaward movement of salt fingers. The models indicate that geologic heterogeneity may explain the lack of field observations of salt fingers in real-world intertidal mixing zones. The findings have implications for predicting the onset of free convection in beaches and for understanding intertidal pore water biogeochemistry and chemical fluxes to the ocean.

1. Introduction

Sandy beaches can discharge substantial quantities of groundwater to the coastal ocean in the form of fresh submarine groundwater discharge (SGD) (Taniguchi et al., 2002). Fresh SGD is a major source of nutrients to the marine environment (Santos et al., 2021; Taniguchi et al., 2019), contributing to eutrophication and water quality degradation, which imposes pressures on coastal marine ecosystems, resources, and economies (Hwang et al., 2005; Michael et al., 2017). For instance, along the Pinellas peninsula in Florida, USA, the magnitude of nitrogen and phosphorous loads in fresh SGD may be 40%–100% of those in river discharge (Kroeger et al., 2007). Similarly, in the Upper Gulf of Thailand, Burnett et al. (2007) estimated that dissolved organic nitrogen and phosphorus groundwater fluxes were 30%–130% of nearby river inputs. In Moune Bay, Japan, Nakajima et al. (2021) found that nutrient concentrations in fresh and saline groundwater discharging to the bay were comparable to or slightly higher than the concentrations in river discharge. Groundwater discharge at the coast can also serve as a source of metals and carbon to marine surface waters (Ahrens et al., 2020; Riedel et al., 2011; Trezzi et al., 2016). Concentrations and thus fluxes of these and other ecologically important solutes are modified along discharging flow paths by biogeochemical reactions in beach saltwater-freshwater mixing zones (Anwar et al., 2014; Charette & Sholkovitz, 2002; Kim et al., 2017; Slomp & Van Cappellen, 2004). Therefore, a better understanding of the conditions that promote or suppress saltwater-freshwater mixing processes in beach aquifers is important for improving groundwater chemical flux estimates along shorelines, which could help inform strategies for reducing anthropogenic contaminant loads to the coastal environment.

Flow and solute transport in coastal groundwater systems is driven by tides (Ataae-Ashtiani et al., 1999; C. Robinson, Li, & Barry, 2007; Vandenbohede & Lebbe, 2006), waves (Geng et al., 2017; Heiss et al., 2015; Sous et al., 2016; Xin et al., 2010), the terrestrial freshwater hydraulic gradient (Heiss & Michael, 2014; Kuan et al., 2019; M. Robinson et al., 1998), and density gradients (Cooper, 1959). In beach aquifers influenced by these physical forcing mechanisms, a shallow saltwater-freshwater mixing zone forms under the intertidal zone (Figure 1a). The mixing zone is separated from the lower saltwater-freshwater interface located farther seaward by a region of discharging fresh groundwater. Convective circulation along the lower interface is driven by the

© 2024. The Authors.

This is an open access article under the terms of the Creative Commons Attribution License, which permits use, distribution and reproduction in any medium, provided the original work is properly cited.

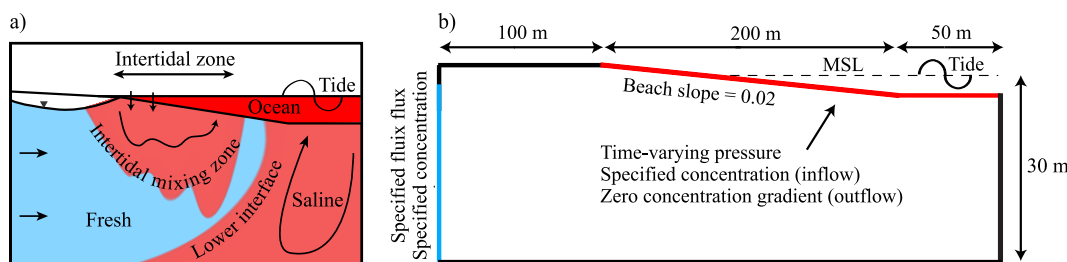


Figure 1. (a) Conceptual model showing an unstable intertidal saltwater-freshwater mixing zone in a tidally-influenced beach aquifer. (b) 2D cross-section of the model domain showing flow and transport boundary conditions.

density contrast between freshwater and saltwater, while flow in the intertidal mixing zone is driven by the hydraulic gradient that forms from the infiltration of seawater across the beachface from tide and wave action, the terrestrial freshwater hydraulic gradient, and in some cases density gradients. The combined influences of terrestrial and marine forcings on the beach flow system produce a distinctive flow configuration whereby seawater infiltrates high on the beachface and flows downward and seaward until it discharges across the seabed, forming a saltwater circulation cell (C. Robinson et al., 2006; Vandebroek & Lebbe, 2006). The size, shape, and geometry of the intertidal mixing zone at the boundaries of the circulation cell are key controls on the intensity and spatial distribution of redox processing of discharging groundwater (Beck et al., 2017; Heiss et al., 2017; Waska et al., 2019). Therefore, knowledge of the physical characteristics of the mixing zone in beaches can provide insight into aquifer reactivity.

The presence of saltwater above less-dense freshwater in the beach subsurface creates a fluid density inversion that promotes unstable flow characterized by free convection and the downward transport of density instabilities, or salt fingers, into the underlying freshwater (Figure 1a) (Greskowiak, 2014; Shen et al., 2019). The formation, prevalence, and size of salt fingers is controlled by the prevailing hydrologic, morphologic, and hydrogeologic conditions. Greskowiak (2014) performed a numerical sensitivity analysis for predicting conditions that generate unstable flow and found that salt fingers may develop in gentle-sloping beaches with a large tidal amplitude, small freshwater flux, and high horizontal hydraulic conductivity (K). System complexity such as beach profile convexity (Y. Zhang et al., 2017), low permeability layers (J. Zhang et al., 2021), multifractal permeability heterogeneity (Geng, Michael, et al., 2020), tidal flooding (Heiss et al., 2022), and time-varying freshwater inflow (Fang, Zheng, Guo, et al., 2022; Fang, Zheng, Wang, et al., 2022) can also affect the likelihood for unstable flow to occur. In systems with unstable flow, the seaward transport and periodic discharge of salt fingers across the aquifer-ocean interface leads to considerable temporal variation in fresh SGD compared to stable mixing zones (Fang et al., 2021; Greskowiak, 2014; Röper et al., 2015). Unstable flow in beach aquifers also affects tide-induced saltwater circulation and density-driven flow along the lower interface (Fang, Zheng, Wang, et al., 2022). The results of the aforementioned studies suggest that salt fingers may form in real beach aquifers under a range of hydrologic forcing and aquifer parameter combinations. However, those studies are based on numerical models or laboratory sand tank experiments.

Salt fingering has rarely been observed in the field despite a substantial body of literature depicting salinity distributions in beaches along the world coastline. We identified 37 field studies showing spatial distributions of pore water salinity in hydrologically, morphologically, and hydrogeologically diverse beach aquifers (Table 1). Three of the studies show fingering flow patterns. Of those three, two reveal fingering flow following inundation from storm surge (Andersen et al., 2005; Xing et al., 2023), and only one study shows persistent unstable conditions (Y. Zhang et al., 2023). Beaches in a number of the other 34 studies have conditions that should promote fingering flow (Table 1). The lack of field observations of fingering flow patterns in beaches reflects a disconnect between theory and reality, suggesting that the conditions required for salt fingering in natural environments are more complex than what has been numerically and physically modeled to-date.

Beach groundwater flow and salt transport dynamics are affected by geologic heterogeneity. Previous groundwater modeling studies of beach aquifers show that geologic heterogeneity intensifies mixing processes due to greater mechanical dispersion (Geng, Boufadel, et al., 2020; Geng, Michael, et al., 2020; Heiss et al., 2020). The intensified mixing occurs in pockets in the subsurface where permeability contrasts between sediment bodies results in shear and deformation of intertidal flow (Geng, Michael, et al., 2020), which, when combined with

Table 1*Field Studies Showing Cross-Sections of Salinity Measured in Beach Aquifers*

Location	Beach slope	Criteria met (Y/N) ^a	Citation
Waquoit Bay, Massachusetts, USA	n/a ^b	N	Abarca et al. (2013)
Magilligan Test Site, northwest Northern Ireland	<0.02	Y	Águila et al. (2022)
Isefjord, Zealand, Denmark	0.02	Y	Andersen et al. (2005)
Esbjerg, Wadden Sea, Denmark	n/a	unknown	Andersen et al. (2007)
Spiekeroog Island, Lower Saxony, Germany	0.04	N	Beck et al. (2017)
Rarotonga, Cook Islands	n/a	unknown	Befus et al. (2013)
The Truc Vert beach, Aquitane, SW France	n/a	unknown	Buquet et al. (2016)
Martinique Beach, Quebec, Canada	0.11	N	Chaillou et al. (2014)
Martinique Beach, Quebec, Canada	0.11	N	Chaillou et al. (2018)
Martinique Beach, Quebec, Canada	n/a	unknown	Couturier et al. (2017)
Spiekeroog Island, Lower Saxony, Germany	0.03	Y	Ehlert et al. (2016)
Moreton Island, Queensland, Australia	0.05	N	Gibbes et al. (2007)
Spiekeroog Island, Lower Saxony, Germany	0.04	N	Grünenbaum et al. (2023)
Cape Henlopen, Delaware, USA	0.11	N	Heiss and Michael (2014)
Waquoit Bay, Massachusetts, USA	n/a	unknown	Henderson et al. (2010)
Cape Shores, Delaware, USA	0.11	N	Kim et al. (2017)
Cape Shores, Delaware, USA	0.10	N	Kim et al. (2022)
Florida State University Marine Laboratory, Gulf of Mexico	0.10	N	Li et al. (2009)
Ting Kok, Tolo Harbour, Hong Kong	0.01	Y	Liu et al. (2017)
Ardeer, near Irvine Bay, Scotland	n/a	unknown	Mao et al. (2006)
Cape Shores, Delaware, USA	0.11	N	McAllister et al. (2015)
Waquoit Bay, Massachusetts, USA	n/a	unknown	Michael et al. (2005)
Spiekeroog Island, Lower Saxony, Germany	n/a	unknown	Reckhardt et al. (2015)
Spiekeroog Island, Lower Saxony, Germany	n/a	unknown	Reckhardt et al. (2017)
Moreton Island, Queensland, Australia	0.05	N	Robinson et al. (2006)
Moreton Island, Queensland, Australia	0.05	N	Robinson, Gibbes, et al. (2007)
Indian River Lagoon, Florida, USA	n/a	unknown	Roy et al. (2013)
Spiekeroog Island, Lower Saxony, Germany	0.03	Y	Seidel et al. (2015)
Martinique Beach, Quebec, Canada	n/a	unknown	Sirois et al. (2018)
Wickford Harbor, Rhode Island, USA	n/a	unknown	Thorn and Urish (2013)
Cape Cod, Massachusetts, USA	n/a	unknown	Urish and McKenna (2004)
Western Belgian coastal plain	0.02	Y	Vandenbohede and Lebbe (2006)
Shilaoren Beach, Shandong Province, China	0.03	Y	Xing et al. (2023)
Werribee River Estuary, Melbourne, Australia	n/a	unknown	Zamora et al. (2021)
Muri Lagoon, East Coast of Rarotonga, Cook Islands	0.10	N	Zhang et al. (2017)
Shilaoren beach, Shandong Province, China	0.02	Y	Zhang et al. (2023)

Note. The Y/N criteria refers to whether field conditions promote unstable flow according to previously published numerical experiments. ^aField sites with a beach slope of equal to or less than 0.03 are considered favorable for unstable flow, as more than half of simulated salinities in the sensitivity analysis of Greskowiak (2014) displayed unstable flow below a slope of 0.03. The conditions for unstable flow are more complex than the criteria assumed here. This table is a first-order estimate of sites where unstable flow may occur. ^bn/a denotes not available.

transient preferential flows over tidal cycles, enhances spreading of contaminant plumes in the beach (Geng, Boufadel, et al., 2020). Greater mixing between fresh and saline groundwater in heterogeneous aquifers can increase nitrate attenuation in discharging fresh groundwater by 80% relative to hydraulically equivalent homogeneous aquifers (Heiss et al., 2020). J. Zhang et al. (2021) investigated mixing in beach aquifers composed of

alternating layers of sand and silt. They found that the presence of a low permeability layer can restrict the downward movement of salt fingers, resulting in a smaller intertidal mixing zone. Evans and Wilson (2017) found that a layer of silt in a beach on Cabretta Island, Georgia, USA resulted in salinity distributions and SGD rates that substantially deviated from those predicted for homogeneous sediments. While the above studies considered the effects of geologic heterogeneity on mixing processes in intertidal aquifers, the focus was on either quantifying local-scale flow deformation or on the impact of layer-cake geology. The role of complex permeability heterogeneity on the stability of the intertidal mixing zone is unclear.

In this study, we hypothesized that complex geologic heterogeneity in beach aquifers inhibits the formation of salt fingers due to higher mechanical dispersion, which leads to lower concentration gradients and a more stable saltwater-freshwater mixing zone. To test this hypothesis, we performed numerical variable-density variably-saturated groundwater flow and salt transport models of tidally-influenced beach aquifers with heterogeneous distributions of sedimentary facies. Specifically, we conducted a sensitivity analysis of intertidal salinity distribution, mixing zone size, and groundwater discharge patterns under varying degrees of heterogeneity and multiple levels of geologic connectivity. Heterogeneous simulations were compared to hydraulically equivalent homogeneous models to isolate the effects of preferential flow conduits on salinity and SGD instability. Our results demonstrate the role of geologic heterogeneity on salt fingering processes and provide a possible explanation for inconsistencies between existing models and observations.

2. Methods

2.1. Geostatistical Modeling

Heterogeneous K realizations of fine and medium sand were generated with unconditional geostatistical simulations using sequential Gaussian simulation algorithm (Deutsch & Journel, 1997) in SGeMS (Remy et al., 2009). Sequential Gaussian simulation creates a randomly distributed assemblage of lithofacies based on a variogram model that describes the spatial correlation of sediment bodies. We used three horizontal variogram ranges (5 m, 12.5 m, and 20 m) and the same vertical variogram range (0.25 m) to generate three groups of 2D shore-perpendicular Gaussian fields. We then truncated the Gaussian fields (see below), resulting in three geologic continuity groups (Figure 2). The horizontal correlation lengths capture a possible range of geologic continuity that may exist in real systems. The spatial scale of the depositional structures is representative of storm deposits, differential sorting on beach cusp horns and embayments, mismatch of native sand and nourished sediment, beachrock, and barrier island migration into marsh sediments and infilled marsh channels.

The proportion of fine sand in each continuity group was increased from 0.1 to 0.9 in increments of 0.2 by truncating the Gaussian values using threshold values corresponding to the targeted proportions of fine and medium sand (Beucher & Renard, 2016), resulting in five proportions of fine sand for the three continuity groups (Figure 2 rows). The varying proportion of fine versus medium sand is indicative of the degree of geologic heterogeneity, K_{Δ} . For instance, an aquifer that is 10% fine sand is composed primarily of medium sand and thus has a low degree of heterogeneity, while an aquifer that is 50% fine sand has high heterogeneity. Beyond 50% fine sand, heterogeneity decreases because the lithology is reversed (medium sand occupies a majority of the subsurface).

Thirty Gaussian fields were simulated for each of the 15 fine sand proportion and geologic continuity combinations (i.e., geologic scenario) to ensure that groundwater model results converged to an acceptable level; considering all models, the size of the intertidal mixing zone converged to within 2% (Figures S1–S15 in Supporting Information S1). A total of 450 K realizations were generated: 3 continuity groups \times 5 fine sand proportions per continuity group \times 30 Gaussian fields for each fine sand proportion and continuity combination. The spatial connectedness and geometric properties of the medium sand facies were quantified with eight metrics (Tables S1a–S1c in Supporting Information S1). The metrics were used to evaluate the impact of facies connectivity and shape on mixing zone stability.

Low-K facies were assigned a K of 2 m/d and high-K facies were assigned a K of 18 m/d, representing fine and medium sand, respectively (Freeze & Cherry, 1979). These values fall within the range of K values reported for sandy beaches in literature (Table 1) and differ by less than one order of magnitude, indicating relatively mild heterogeneity for the cases considered in this study. The K values were also chosen such that the effective

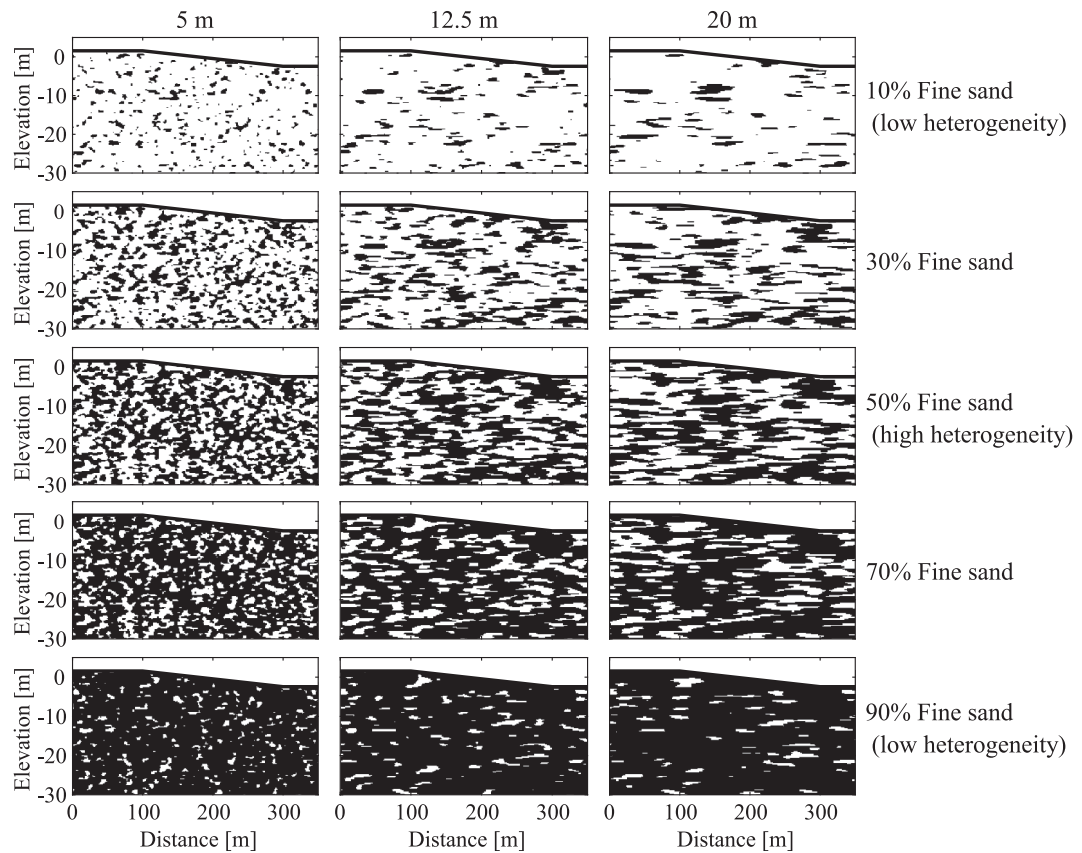


Figure 2. Example heterogeneous K fields for three geologic continuity groups (horizontal variogram ranges; columns) and five proportions of fine sand (rows). The aquifer sediment is composed of fine (black) and medium (white) sand.

hydraulic properties of geologic scenarios consisting of 50% fine sand and 50% medium sand were equivalent to the homogeneous base case model (see Section 2.2).

Fifteen hydraulically equivalent homogeneous simulations were performed to understand salt finger formation in anisotropic systems. The homogeneous models were assigned effective hydraulic conductivity values equivalent to the heterogeneous cases. The effective horizontal ($K_{X,\text{eff}}$) and vertical ($K_{Z,\text{eff}}$) K values were obtained from the heterogeneous cases by simulating groundwater flow horizontally and vertically through the model domain. Darcy's law was used with the simulated fluxes to calculate equivalent effective K values for the 450 realizations (Supporting Information Tables S2a–S2c in Supporting Information S1). This approach for estimating effective K values assumes that the principle direction of permeability is parallel to the X and Z direction. The average horizontal and vertical K values across the 30 realizations for each of the 15 combinations of fine sand proportion and geologic continuity were assigned to the 15 hydraulically equivalent homogeneous models.

2.2. Numerical Modeling

Transient variable-density variably-saturated flow and salt transport was simulated through the 450 heterogeneous realizations and 15 homogeneous cases with the subsurface flow and reactive transport code PFLOTRAN (Lichtner et al., 2015). PFLOTRAN has been widely used for modeling surface-subsurface exchange of water, heat, and solutes (e.g., Chen et al., 2022; Dwivedi et al., 2018; Peng et al., 2023; Song et al., 2018; Wallace et al., 2020). Variable-density flow in PFLOTRAN is solved using the Richards equation (Richards, 1931), which is coupled to salt transport with the advection-dispersion equation. The van Genuchten formula (Van Genuchten, 1980) is used to relate pressure to saturation, and the Mualem equation (Mualem, 1976) describes relative permeability from saturation. Fluid density is calculated as a function of salinity, pressure, and temperature following the Batzle and Wang (1992) equation of state.

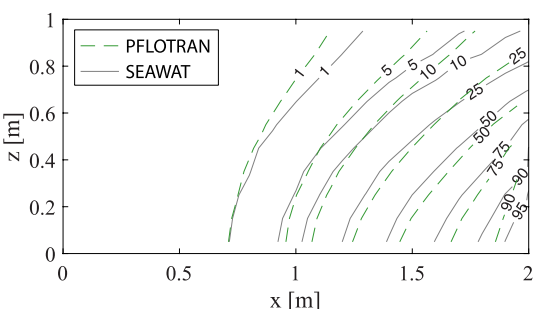


Figure 3. PFLOTRAN verification showing percent seawater salinity contours for the benchmark Henry problem.

We are not aware of any previous study that has validated PFLOTRAN for simulating variable-density flow and salinity distributions in coastal aquifers; therefore, we validated PFLOTRAN for such a purpose. For validation, we used the benchmark Henry problem (Henry, 1964), which has been employed for verifying commonly used variable-density numerical codes (e.g., Langevin et al., 2008; Voss & Provost, 2010). Briefly, the Henry problem is a rectangular ($2 \text{ m} \times 1 \text{ m} \times 1 \text{ m}$) 2D cross-sectional model with saltwater intrusion on the vertical right side of the model and freshwater inflow on the left side of the domain. The left boundary is assigned a constant influx of fresh groundwater with a salinity of 0 ppt, representing terrestrial recharge. The right boundary is a prescribed hydrostatic pressure accounting for the density of seawater. Inflow into the model from the right boundary has a salt concentration equal to seawater, and outflowing water along the boundary has a

concentration of the ambient groundwater. The top and bottom boundaries are impermeable. Comparison of simulation results from PFLOTRAN and the variable-density flow code SEAWAT v4 (Langevin et al., 2008) is shown in Figure 3. The relative salt concentration contours are in good agreement. While there are some offsets, they are expected because PFLOTRAN uses a nonlinear equation of state that is more complex than the equation of state implemented in SEAWAT, which assumes a linear relation between salt concentration and fluid density.

The model domain in this study represented a shore-perpendicular cross-section of a tidally-influenced coastal aquifer. The base case model domain and parameters were adopted from the base case scenario of Gresko-wiak (2014). The model extended 30 m below mean sea level (MSL) and 2 m above MSL. The landward vertical boundary was 200 m inland of the beachface-MSL intersection and the seaward vertical boundary was 150 m offshore (Figure 1; right panel). The base case model was homogeneous and isotropic and its parameters were specifically chosen to promote unstable flow: $K = 10 \text{ m/d}$, tidal amplitude (A) = 1.5 m, freshwater inflow (Q_f) = $2.1 \text{ m}^3/\text{d}$, beach slope (β) = 0.02, longitudinal dispersivity (α_L) = 0.5 m, and transverse dispersivity (α_T) = 5×10^{-4} m. These parameter values allowed us to evaluate whether induced dispersion from geologic heterogeneity can diminish fingering flow even under conditions that strongly encourage free convection. In heterogeneous models, K varied spatially according to the distribution of the fine and medium sand lithofacies generated from the geostatistical models. With the exception of K and the landward vertical boundary condition, the base case setup was used in the heterogeneous and homogeneous models. This means the same dispersivity values were assigned to the homogeneous and heterogeneous models. The implications of this are discussed in Section 4.3.

The model domain was discretized with prismatic elements that ranged in size from 0.25 m at the aquifer-ocean interface to 1.00 m at the base of the model domain. Mesh discretization tests were performed to ensure that model results were independent of element size and absent of numerical dispersion. The flow timestep size was 30 min to resolve tidal fluctuations. Models were run to five and a half years after achieving dynamic-steady state with respect to salt concentrations.

2.3. Boundary Conditions

The model boundary conditions captured the key hydrologic forcings acting on a beach aquifer. In the heterogeneous models, terrestrially-derived fresh water inflow was represented as a specified hydraulic head of 2.0 m along the landward vertical boundary. The simulated freshwater fluxes in the heterogeneous models were assigned to each corresponding homogeneous model to ensure equivalency. A semidiurnal tide was applied along the beachface and seabed by specifying a sinusoidal time-varying hydraulic head boundary:

$$h(t) = A \cos(\omega t) \quad (1)$$

where h [L] is the tide elevation varying with time t [T]. A [L] is the tidal amplitude, ω [$\deg T^{-1}$] is the tidal angular frequency ($\omega = 2\pi/T$, where T is tidal period = 12.57 hr). A seepage face boundary condition was implemented along the ocean boundary to allow groundwater to discharge above the tide level. The storage and release of water due to sediment compressibility (Reeves et al., 2000; Wilson & Gardner, 2006) was not considered because numerical tests have shown that the effects of compressibility on flow through tidally-influenced coastal

sediments is negligible when the hydraulic conductivity is greater than 10^{-6} m/s (Xin et al., 2009), and the K values in the present study are several orders of magnitude higher than this threshold value.

The ocean boundary was assigned a zero-concentration gradient boundary condition in which inflowing portions along the aquifer-ocean interface were assigned a salt concentration of 35 ppt representing seawater, while salinity of groundwater flowing out of the aquifer had a concentration of the ambient pore water at the boundary. The salt concentration at the inland vertical boundary was specified as 0 ppt. All other boundaries were assigned as zero salt mass flux.

2.4. Assessment Metrics

Several quantitative metrics were employed to evaluate how system stability responded to geologic heterogeneity. The intertidal *mixing zone area* was defined as the cross-sectional area where pore water was between 10% and 90% seawater, less the area of the lower saltwater-freshwater interface in the base case without tides. Mixing zone size was calculated by integrating the areas of all elements with salinities between 10% and 90% seawater. Greskowiak (2014) introduced the concept of nondimensional $\varepsilon-\pi_1$ space for mapping conditions for salt finger formation, where ε (Schincariol et al., 1994) is a perturbation parameter and π_1 (Oostrom et al., 1992) is a reflection of the buoyancy effect in variable-density systems. The perturbation parameter ε describes the effect of tides on periodically perturbing heads and concentrations in the intertidal saltwater-freshwater mixing zone, which can initiate unstable flow. ε is defined following Robinson, Li, and Prommer (2007) and Greskowiak (2014):

$$\varepsilon = \frac{A}{S_b} \sqrt{\frac{n_e \omega}{2K_H B}} \quad (2)$$

where A [L] is the tidal amplitude, S_b [–] is the beach slope, n_e [–] is the effective porosity, ω [deg T^{-1}] is the tidal angular frequency, K_H [L/T] is the horizontal hydraulic conductivity, and B [L] is the aquifer thickness. High ε signifies a strong tidally-driven perturbation and a higher likelihood for unstable flow. Greskowiak (2014) showed that ε alone is insufficient for predicting unstable flow; however, ε can be used with π_1 to create a 2D parameter space where the onset of density fingering can be more reliably predicted. π_1 is given by (Oostrom et al., 1992):

$$\pi_1 = \frac{K_V \Delta \rho}{q_f \rho_f} \quad (3)$$

where K_V [L/T] is the vertical hydraulic conductivity, $\Delta \rho$ [M/L^3] is the difference in density between saltwater and freshwater, q_f [L/T] is the Darcy flux in the intertidal mixing zone, and ρ_f [M/L^3] is the density of freshwater. In tidally-influenced beaches, q_f varies temporally and spatially within the mixing zone, thus we take q_f as Q_f/B (Fang et al., 2022a, 2022b; Greskowiak, 2014). We computed ε and π_1 for each heterogeneous model using the effective horizontal and vertical hydraulic conductivities. Stable and unstable flow conditions were then mapped in $\varepsilon-\pi_1$ space and evaluated against previously published stability criteria for homogeneous beach aquifers.

Fresh SGD hereafter is defined as the tidally-averaged fresh discharge rate across the aquifer-ocean interface. Fresh SGD was calculated by multiplying the total discharge rate at each model element along the ocean boundary by the fraction of freshwater at the element, and integrating along the boundary at each time step. A running average with a period of one tidal cycle was applied to the instantaneous fresh discharge rates to obtain tidally-averaged fresh discharge.

3. Results

3.1. Effects of Geologic Heterogeneity on System Stability

The simulated salinity distributions in the heterogeneous models diverged markedly from the base case and showed a clear influence of geology on salt finger formation. As expected, the salinity distribution in the base case model indicated unstable flow characterized by the fingering flow pattern (Figure 4). Density fingers emerged from the ocean side of circulation cell and moved downward and seaward, consistent with the simulation results

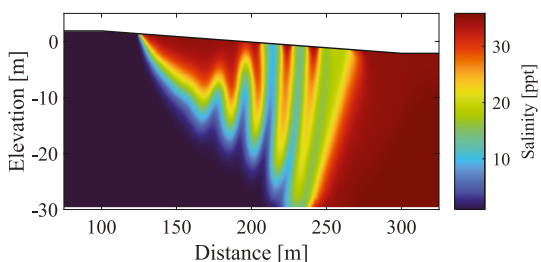


Figure 4. Salinity distribution in the base case scenario.

brackish at depth and areas seaward. Salinity distributions in several of the models with stable flow (e.g., Figure 5 row 4, column 1 and 2) depicted some characteristics of fingering flow. However, those vertical protrusions were at steady-state and were the result of advective transport from downward flow of circulating saltwater within preferential flow paths rather than forming from buoyancy forces.

Unstable flow occurred in all hydraulically equivalent homogeneous models. Comparison between the heterogeneous (Figure 5) and homogeneous (Figure 6) models illustrates that unstable flow was inhibited by spatial

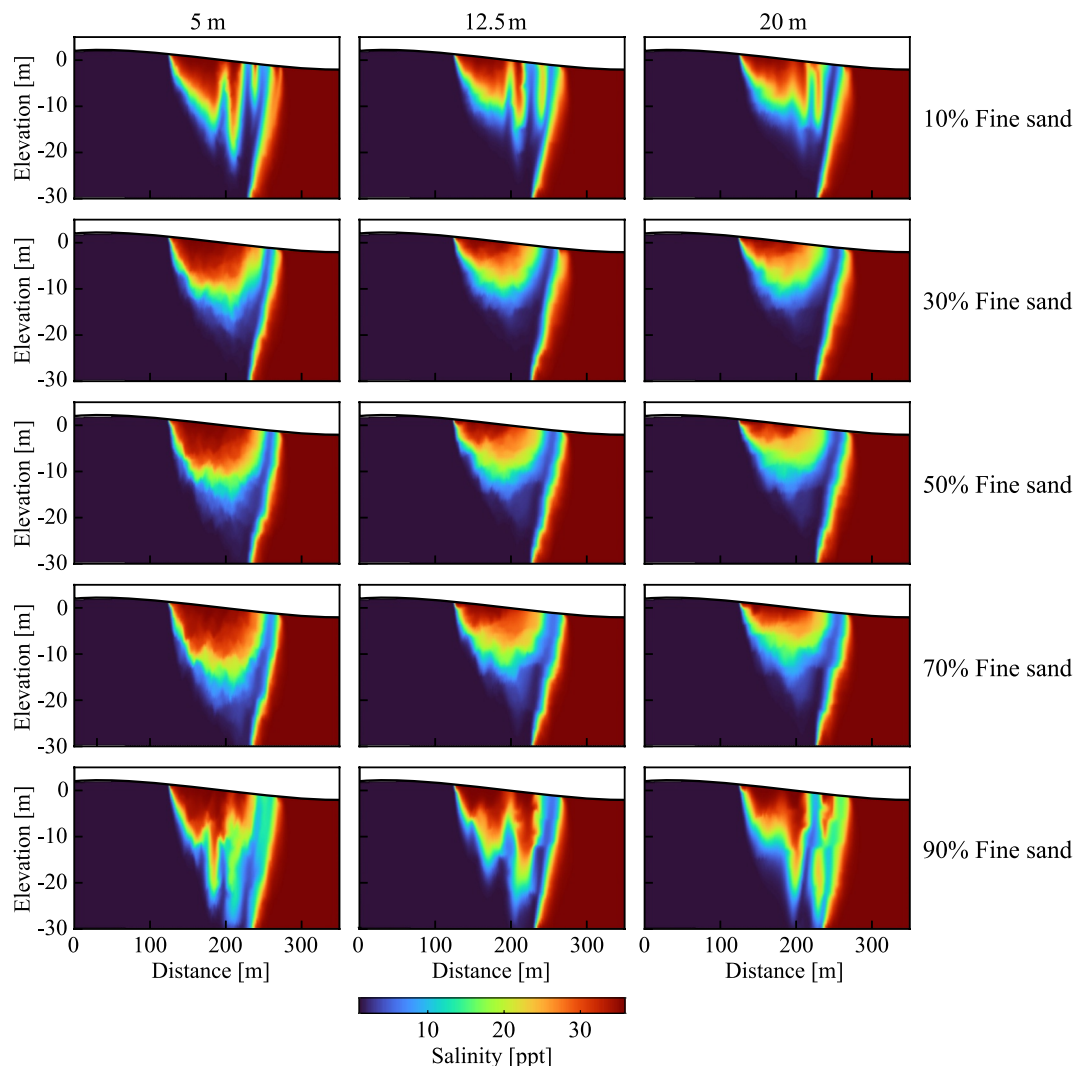


Figure 5. Simulated salinity distributions for example heterogeneous models for the three horizontal variogram ranges (columns) and five proportions of fine sand (rows).

of Greskowiak (2014). The saltwater fingers, of which there were generally 3–5 present at any moment in time, often penetrated to the base of the aquifer before coalescing with the density-driven saltwater interface in the subtidal zone.

Conversely in the heterogeneous aquifers, salt fingers did not form in sediments consisting of 30%, 50%, or 70% fine sand (Figure 5 rows 2–4). This was the case for all three geologic continuity groups for the 30%–70% fine sand proportions. The intertidal mixing zone in these models had weaker concentration gradients; there was a comparatively gradual transition of salt concentrations from high salinity under the center of the beachface to fresh-

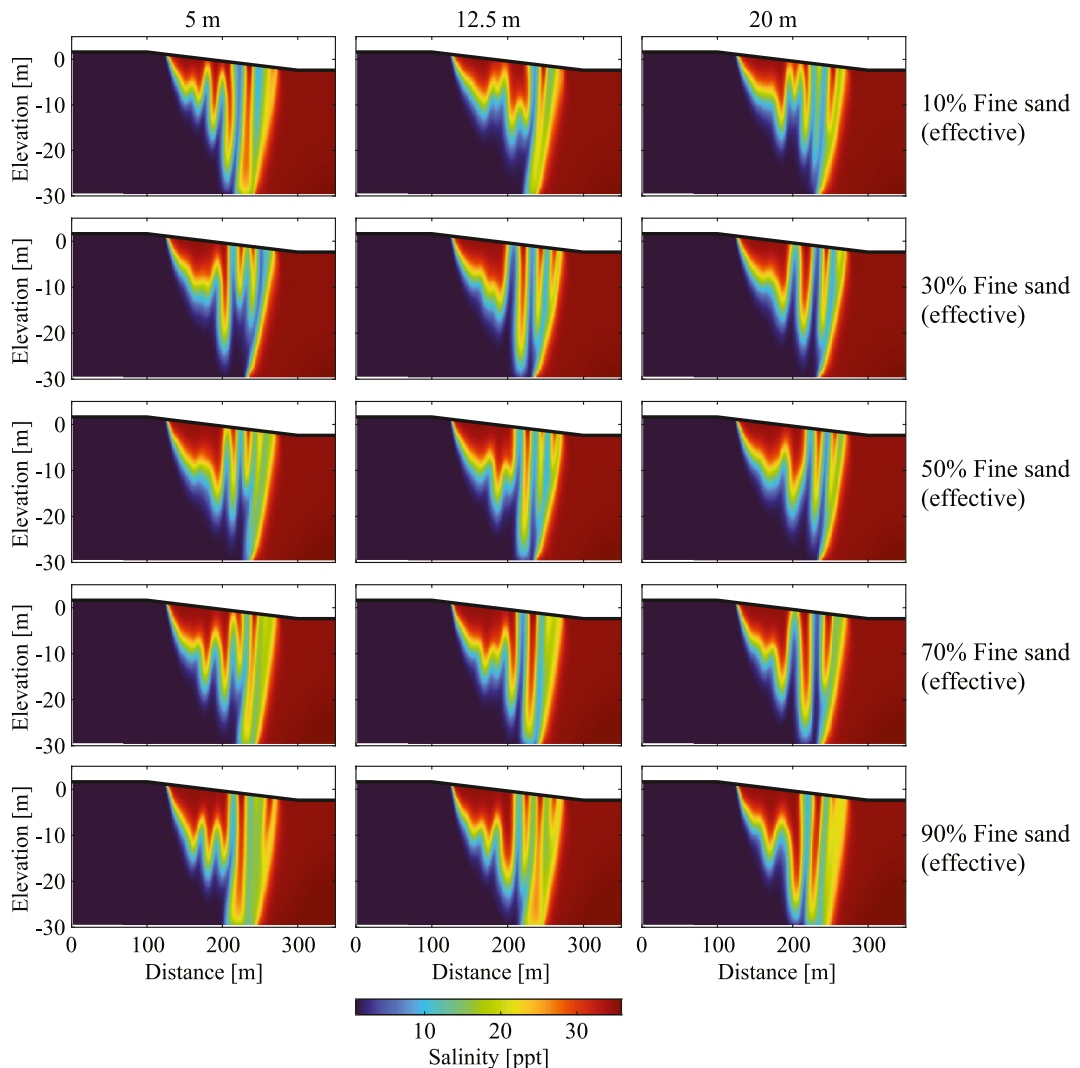


Figure 6. Simulated salinity distributions for the hydraulically equivalent homogeneous models for the three horizontal variogram ranges (columns) and the five effective proportions of fine sand (rows).

variability in hydraulic conductivity for the 30%–70% fine sand proportions. This was due to enhanced dispersion resulting from the complex geologic structure in the heterogeneous models. More intense mixing reduced density gradients, which created a stable circulation cell absent of salt fingers. System stability was accompanied by a single fresh discharge zone (Figure 5), whereas multiple evolving fresh-brackish discharge zones formed in the hydraulically equivalent homogeneous models (Figure 6).

Density fingers developed in heterogeneous models with 10% and 90% fine sand owing to the low degree of heterogeneity in those models (Figure 5 rows 1 and 5). The 10% and 90% proportions have the same relative degree of heterogeneity because the sediment compositions are simply reversed (this is also the case for the 30% and 70% fine sand proportions). Like the homogeneous and base case simulations, the salt fingers in simulations with the 10% and 90% proportions emerged from the ocean-side of the circulation cell; however, the finger protrusions were less well-defined, generally smaller, and more irregularly shaped than the homogeneous counterparts (Figures 5 and 6). For instance, at high geologic connectivity and 90% fine sand (Figure 5 row 5, column 3), a salt finger at $x = 240$ m was split in two by a high-K unit at 10 m depth. The high-K unit acted as a preferential flow pathway that allowed ambient freshwater immediately landward of the instability to converge seaward, bisecting the plume. Similarly, in a model with intermediate connectivity and 90% fine sand (Figure 5

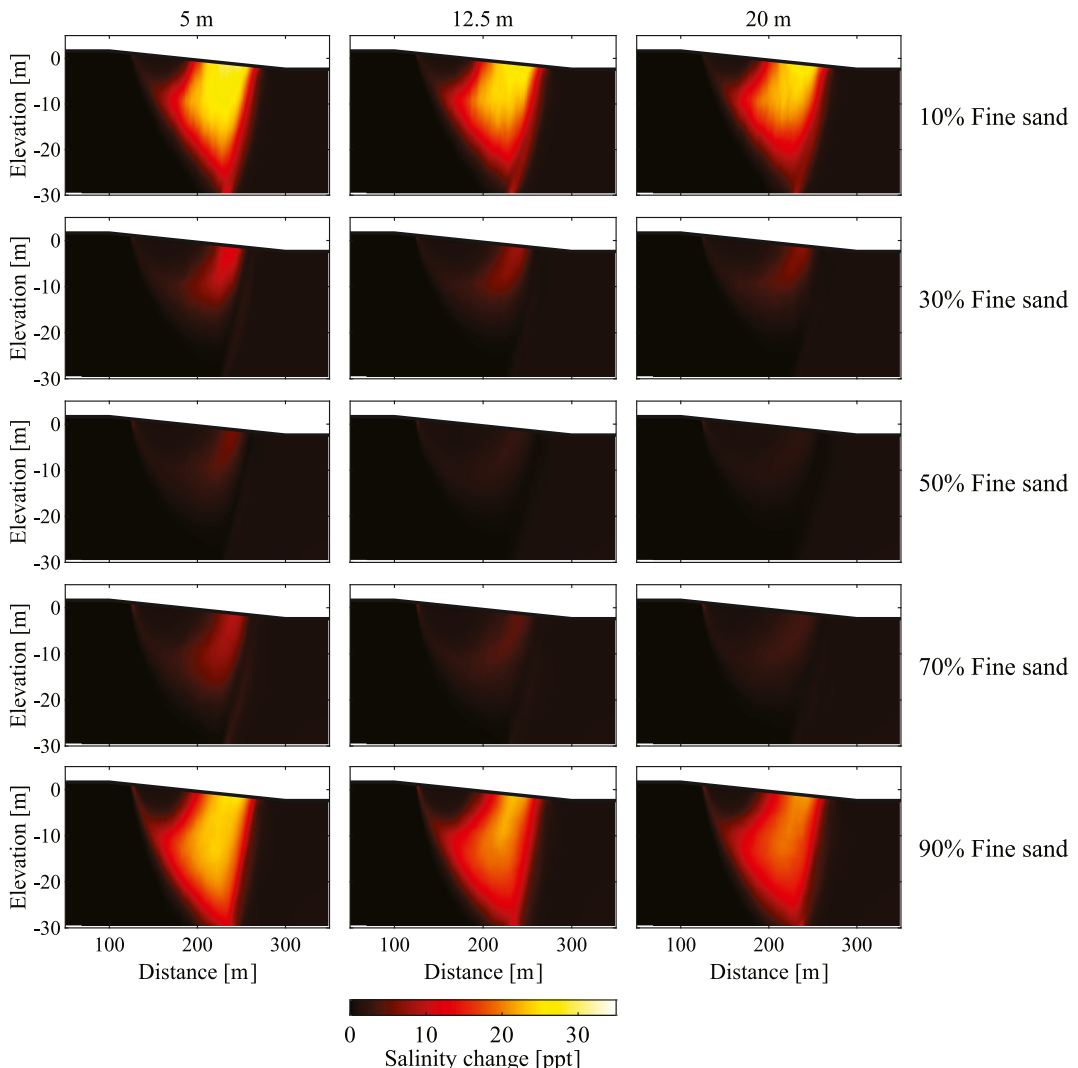


Figure 7. Ensemble-averaged change in salinity at each model element over the 5.5-year simulation period. The salinities shown are for the heterogeneous models for the three horizontal variogram ranges (columns) and five proportions of fine sand (rows).

row 5, column 2), geologic heterogeneity formed pockets of brackish pore water that were imbedded along the perimeter of a salt finger at $x = 210$ m.

3.2. Effects of Geologic Heterogeneity and Connectivity on Salinity Variability

There was a clear relationship between the degree of heterogeneity and changes in salinity over time. Figure 7 shows how ensemble-averaged salinity varied spatially through time for the 15 combinations of geologic continuity and fine sand proportion. Across the three geologic continuity groups, ensemble-averaged changes in salinity were highest in models with 10% and 90% fine sand (low degree of heterogeneity); salinity varied up to 27–30 ppt for sediments with 10% fine sand and 21–24 ppt for sediments consisting of 90% fine sand (Figure 7 rows 1 and 5). Large salinity fluctuations in these simulations extended from the sand surface to 20 m depth or greater in some instances and are consistent with the alternating transport of finger-like columns of freshwater and saltwater seaward. In the same models, salinity was nearly unchanged in the shallow aquifer beneath the upper beachface. Here, salinity remained high throughout the simulation period owing to the continuous infiltration of seawater into the subsurface, forming a crescent-shaped area where salinity changed by less than 1 ppt. Changes in salinity were substantially lower throughout the aquifer for the 30% and 70% fine sand proportions (moderate degree of heterogeneity), where the maximum change was 8–13 ppt and 3–9 ppt, respectively (Figure 7 rows 2

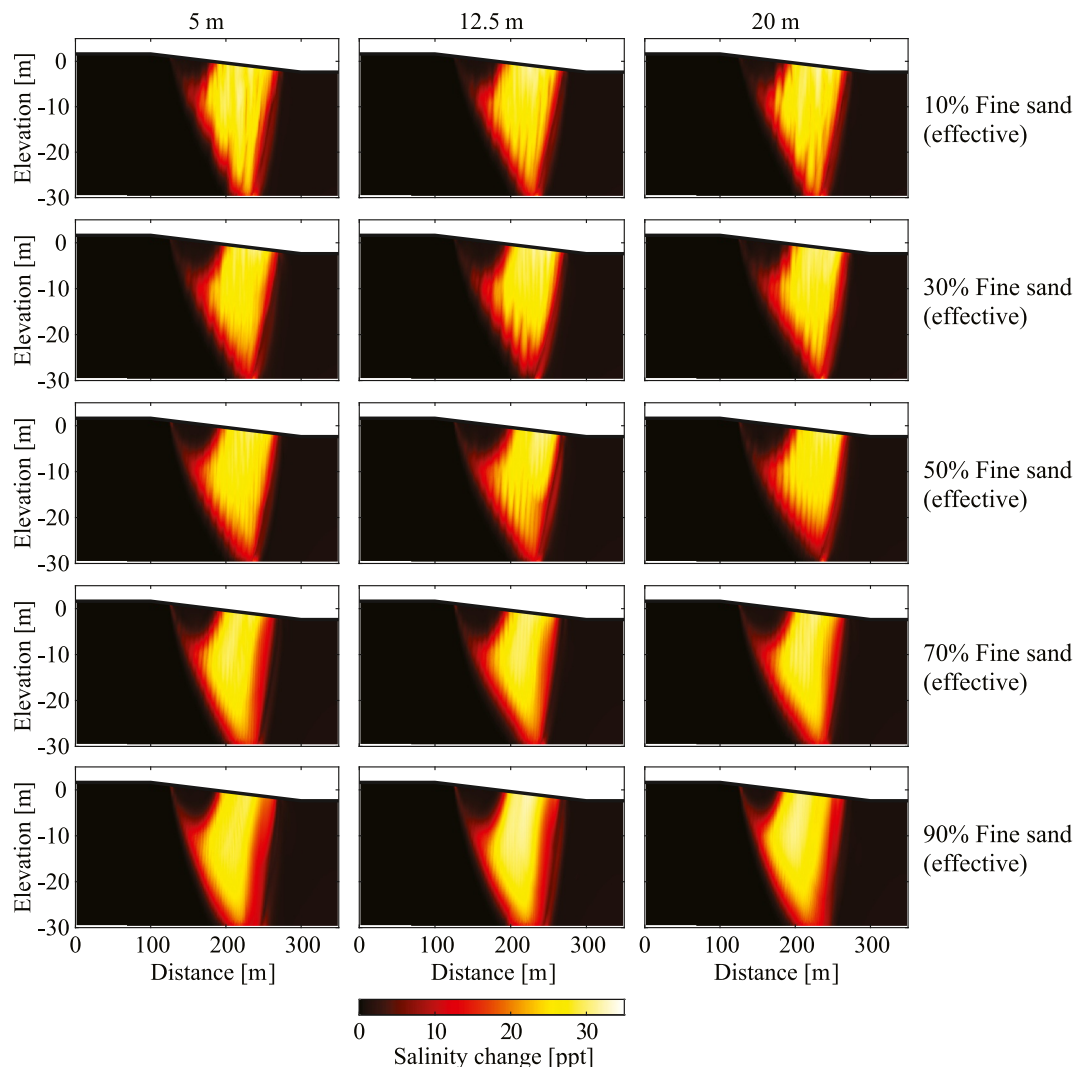


Figure 8. Change in salinity at each model element over the 5.5-year simulation period. The salinities shown are for the hydraulically equivalent homogeneous models for the three horizontal variogram ranges (columns) and five proportions of fine sand (rows).

and 4). Sediments with 50% fine sand (high degree of heterogeneity) produced the smallest salinity changes, reaching to only 2–4 ppt immediately below the low tide line and <1 ppt in the broader mixing zone (Figure 7 row 3).

Although salinity in the 30%–70% proportions did vary beneath the lower beachface (Figure 7 rows 2–4), the changes were not the result of significant salt finger formation, as was the case in the 10% and 90% proportions. Instead, the salinity changes were generated by low-frequency buoyancy-driven expansion and contraction episodes on the seaward side of the circulation cell, resulting in the relatively small salinity changes shown in Figure 7 rows 2–4. The inverse relationship between the degree of heterogeneity and changes in salinity shows that the circulation cell became more stable as heterogeneity and thus dispersion increased. In contrast, salinity varied by no less than 30 ppt across all homogeneous simulations due to widespread fingering flow (Figure 8). These simulation results indicate that the degree of heterogeneity is a key control on system stability, while the influence of anisotropy, as indicated by the homogeneous models, is comparatively negligible.

Geologic continuity had a moderate effect on salinity change. The columns in Figure 7 show that there was a slight decrease in changes in salinity as geologic continuity increased. For example, salinity varied up to 13 ppt for cases with 30% fine sand and low geologic continuity (Figure 7 row 2, column 1), which decreased to 8 ppt

under high continuity (Figure 7 row 2, column 3). A trend of a similar magnitude was evident in the other fine sand proportions. Because the length of medium sand (high-K) bodies increased with geologic continuity (horizontal variogram range) (Tables S1a–S1c in Supporting Information S1), this implies that facies with more connected structure are more effective at enhancing dispersion in the mixing zone, thereby promoting system stability.

A point of consideration is that geologic continuity is also controlled by the proportion of fine sand. The length of high-K bodies decreased as the proportion of fine sand increased from 10% to 90% (Tables S1a–S1c in Supporting Information S1). This is expected because the high-K bodies shrink in size and become discontinuous as low-K material occupies a larger portion of the aquifer. The decrease in high-K continuity from 10% to 50% fine sand corresponded with an increasingly stable mixing zone, becoming most stable at 50% fine sand (Figure 7). Conversely, when high-K continuity was decreased by lowering the horizontal variogram range, the mixing zone became less stable. This is shown in Figure 7 by higher salinity variability in column one compared to columns two and three. These two contrasting responses of mixing zone stability indicate that the trend in stability across the fine sand proportions was not a result of differences in continuity. This is because the horizontal variogram range affects only continuity, and the role of the horizontal variogram range on stability was opposite of that observed in models with varying amounts of fine sand. Thus, although both continuity and the degree of heterogeneity change with the proportion of fine sand, the degree of heterogeneity was the controlling factor on mixing zone stability.

3.3. Time-Averaged Mixing Zone Size

While models with 50% fine sand resulted the most stable intertidal mixing zone, sediments composed of 30% fine sand yielded the smallest mixing area for all three geologic continuity groups (Figure 9). This may be explained by the competing effects of dispersion on mixing zone size in heterogeneous beach aquifers prone to unstable flow. Moderate to high degree of heterogeneity (30%–50% fine sand) greatly enhanced dispersion, which substantially reduced buoyancy-driven flows. This had a shrinking effect on the mixing zone size owing to the absence of fingering flow. However, enhanced mixing from higher dispersion can counteract the shrinking effect. The degree of heterogeneity in both the 30% and 50% proportions was sufficient for eliminating fingering flow, but greater heterogeneity in the 50% proportions generated more dispersion, forming a larger mixing zone.

The size of the mixing zone increased as the fine sand proportion increased from 30% to 90% (Figure 9). For the low continuity group (Figure 9a), the area increased 41% from an average of $1,327 \text{ m}^2$ (30% fine sand) to $1,871 \text{ m}^2$ (90% fine sand). This trend was similar across the three continuity groups. Models with sediments composed of 10% fine sand produced mixing zones with sizes that were between those of the 50% and 70% proportions (Figure 9), further demonstrating the competing controls of enhanced dispersion and salt finger inhibition on mixing area, as discussed above. Mixing zones in the heterogeneous models were on average 22% smaller (max = 29%, min = 15%) than their homogeneous counterparts owing to a reduction in the downward convection of salt (Figure 9 black circles vs. green stars).

Geologic continuity had a minor influence on mixing zone size. The mixing area was on average 7% smaller in high continuity groups relative to low continuity groups (Figure 9a vs. 9c; black circles). This again shows that sediments with greater horizontal connectivity are somewhat more effective at enhancing dispersion in beaches prone to unstable flow, likely due to stronger impediment of vertical flows associated with density fingering.

3.4. Mixing Zone Size Variability Over Time

The degree of heterogeneity strongly controlled the temporal variability in mixing zone size (Figure 10). The smallest oscillations in mixing zone size over the 5.5-year simulation period were in models with 30%–70% fine sand. The size of the oscillations in those models was 36, 59, and 74 m^2 for the 50%, 70%, 30% fine sand proportions, respectively, which is equivalent to 3%, 4%, and 6% of the mixing zone size in those models. These oscillations in mixing zone size compare to an average oscillation of 308 m^2 in the homogeneous cases (Figure 10 black circles vs. green stars). Thus, oscillations in mixing zone size for the 50% fine sand proportion (36 m^2) were eight times smaller than the average oscillation across the hydraulically equivalent set of homogeneous models. Compared to the stable models with 30%–70% fine sand, oscillations in mixing zone size were considerably larger

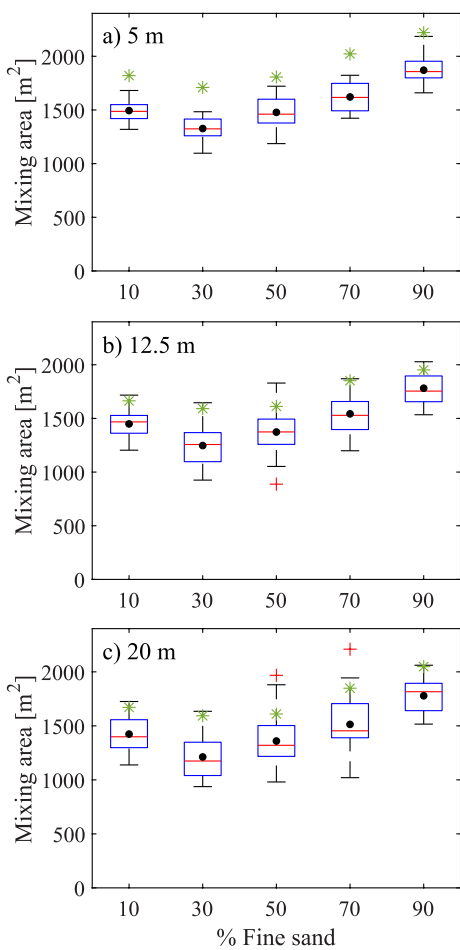


Figure 9. Intertidal mixing zone size for the heterogeneous and hydraulically equivalent homogeneous models for the three horizontal variogram ranges ((a) 5 m, (b) 12.5 m, and (c) 20 m). The reported sizes are the average over the 5.5-year simulation period. In the heterogeneous cases, the box and whiskers for each fine sand proportion are based on their respective 30 ensemble members. The red horizontal lines are the median, the black circles are the mean, the bottom and top edges of the boxes are the 25th and 75th percentiles, respectively, and the whiskers are the maximum and minimum values that are not outliers. The red crosses are outliers (1.5X above or below the interquartile range). The green stars are the equivalent homogeneous models.

4. Discussion

This study provides a possible explanation for the lack of field observations of unstable flow in beach aquifers despite a growing body of literature depicting salinity distributions in beaches worldwide (Table 1). Our results indicate that complex geologic heterogeneity dampens salt finger formation in beaches due to enhanced dispersion, which counteracts the density gradients necessary for free convection. The hydraulic conductivity contrast between the two facies types considered in this study was less than one order of magnitude, implying that even mild heterogeneity can significantly diminish fingering flow in these systems. The finding of suppressed fingering flow in heterogeneous beach sediments contrasts with simulation results of Geng et al. (2020a, 2020b) who showed that heterogeneity amplified the likelihood of unstable flow in the intertidal zone. A possible explanation for the differences is that the styles of heterogeneity differed, and certain styles of heterogeneity support unstable conditions, whereas others do not (Simmons et al., 2001). Vertically oriented high-K zones

in the 10% and 90% proportions, where the mixing zone fluctuated 312 and 203 m² (21% and 11% of mixing zone size, respectively) (Figure 10).

In addition to the magnitude of heterogeneity also affected the frequency at which the mixing zone oscillated. The frequency of the oscillations decreased with increasing heterogeneity (Figure 11); the mixing zone expanded and contracted more frequently in the 10% and 90% proportions compared to the 50% proportion because of convective flow in sediments composed of 10% and 90% fine sand.

3.5. Fresh SGD

Heterogeneity affected temporal variations in fresh SGD. Tidally-averaged fresh SGD was highly variable over time in heterogeneous sediments composed of 10% fine sand and in the 10% (effective) fine sand homogeneous models (Figure 12). Figure 12 shows this was the case in both low (row 1) and high (row 2) continuity scenarios. In the homogeneous models, temporal variability in discharge decreased from an average of 1.71 to 0.23 m³/d as the effective proportion of fine sand increased from 10% to 90% (Figure 13; dashed lines). This compares to a decrease of an average of 1.24 to 0.07 m³/d in the heterogeneous models (Figure 13; solid lines). Within these trends, there were two key differences between the heterogeneous and homogeneous models. First, in heterogeneous sediments with 10%–70% fine sand, discharge varied 19%–86% less compared to the hydraulically equivalent homogeneous models (Figure 13; solid vs. dashed lines) because the more stable intertidal flow patterns in the heterogeneous models produced more steady fresh SGD. Second, the 50% fine sand proportion (high heterogeneity) in the heterogeneous models resulted in the most stable fresh SGD rates (Figure 13 solid lines), varying 86% less than the hydraulically equivalent homogeneous models. Notably, in the example high continuity heterogeneous case shown in Figure 12b, discharge was invariant for the 50% proportion, as shown by the horizontal line representing 50% fine sand. This contrasts with the homogeneous simulations, where the lowest temporal variability in discharge was in sediments with properties equivalent to 90% fine sand (Figure 12 column 2; Figure 13 dashed lines).

For the 10%–50% proportions, more connected geologic structure resulted in fresh SGD was that was more temporally stable. Aquifers with high continuity had discharge rates that were 19% less variable than the low continuity cases (Figure 13 gray vs. black solid lines). The effects of the degree of heterogeneity and geologic continuity on temporal discharge patterns were minor to negligible in sediments with 70%–90% fine sand, as shown by the coincident symbols in Figure 13.

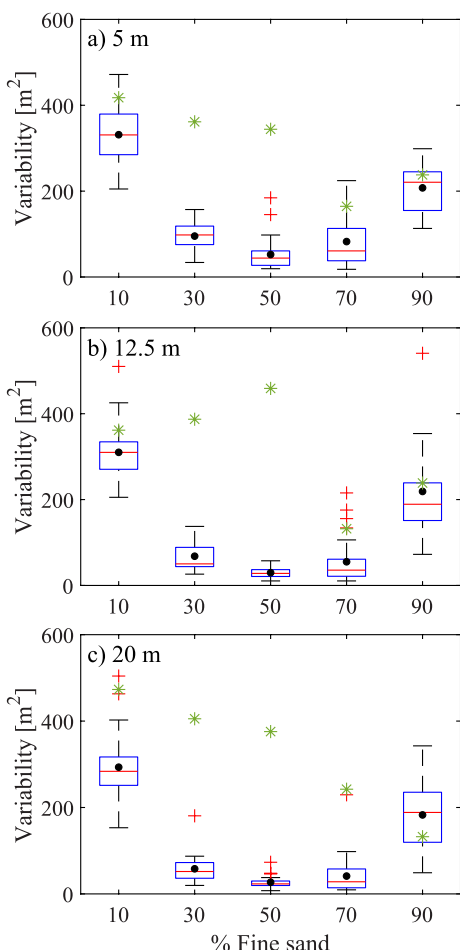


Figure 10. Variability of intertidal mixing zone size for the heterogeneous and hydraulically equivalent homogeneous models for the three horizontal variogram ranges ((a) 5 m, (b) 12.5 m, and (c) 20 m). Variability was calculated as the difference between the maximum and minimum mixing zone area over the 5.5 year simulation period (see Figure 11 time series). In the heterogeneous cases, the box and whiskers for each fine sand proportion are based on their respective 30 ensemble members. The red horizontal lines are the median, the black circles are the mean, the bottom and top edges of the boxes are the 25th and 75th percentiles, respectively, and the whiskers are the maximum and minimum values that are not outliers. The red crosses are outliers (1.5X above or below the interquartile range). The green stars are the equivalent homogeneous models.

enhance instability growth conditions, while lenticular low-K structures and increased spatial variance in K create barriers to the vertical flow required to maintain convection (Simmons et al., 2001). This means heterogeneity exerts two opposing effects on system stability; it can trigger the onset of instabilities and can simultaneously control whether instabilities will grow or decay once formed (Schincariol et al., 1997; Simmons et al., 2001). Thus, differences in styles of heterogeneity between the study herein and Geng et al. (2020a, 2020b) may explain the contrasting model results. More specifically, properties of the K realizations in Geng et al. (2020a, 2020b) may have been more effective at triggering instabilities than dampening their growth, while the opposite appears to have been the case for the realizations considered in the present study.

4.1. Onset of Convective Instability

Across two-dimensional $\epsilon-\pi_1$ space, we compare the onset of fingering flow in our heterogeneous models to fingering flow criteria defined for previously published homogeneous models. As shown by Greskowiak (2014), unstable flow in homogeneous beach sediments is likely for higher values of ϵ and π_1 (Figure 14; light red circles). Greskowiak (2014) also demonstrated that the stable-unstable boundary is a transition zone, which is indicated by the overlapping region of light red and light blue circles in Figure 14. When our ensemble heterogeneous models are plotted in $\epsilon-\pi_1$ space, stable mixing zones (Figure 14; blue triangles) extend beyond the transition zone into the unstable region of the diagram. Specifically, the three vertical groups of blue triangles in Figure 14 are, from left to right, stable mixing zones in heterogeneous models with 30%, 50%, and 70% fine sand. The mapped locations of these stable cases relative to the stable region defined by homogeneous models shows that the onset of stable flow occurs at higher values of ϵ and π_1 for beach aquifers with moderate to high heterogeneity. This implies that mixing zones in heterogeneous systems can be stable under a range of conditions beyond those considered in the present study; conditions that would otherwise generate salt fingers in homogeneous sediments.

Models with low heterogeneity were unstable and thus map correctly within the unstable region of the stability diagram (Figure 14; red triangles). These unstable heterogeneous models were clustered with the stable heterogeneous cases of moderate to high heterogeneity. Thus, for improving prediction of the onset of unstable flow it may be useful to consider the degree of heterogeneity, K_Δ , as a third dimension surrounding $\epsilon-\pi_1$ space. In systems with geologic architecture similar to that considered here, stable mixing zones are more likely for high K_Δ and low ϵ and π_1 . The degree of heterogeneity may alternatively be represented in the stability diagram with an effective dispersivity coefficient that captures macrodispersion in heterogeneous sediments.

The model parameters used in this study (e.g., beach slope, tidal amplitude, and freshwater flux) promote fingering flow. Therefore, owing to the difficulty of measuring detailed K distributions in intertidal zones at high spatial resolution, assessing whether unstable flow patterns exist at a particular site is likely to remain challenging even if the beach profile and hydrologic forcing conditions encourage free convection.

4.2. Implications for Chemical Reactivity and Fluxes

The results of this study have implications for the biogeochemistry of beach aquifers and for chemical fluxes to coastal ocean ecosystems. Many field studies have shown that mixing between freshwater and saltwater is an important control on the spatial extent and magnitude of chemical reactions in intertidal sediments. Notably, field measurements by Kim et al. (2017), McAllister et al. (2015), and Roy et al. (2010) showed that the intertidal

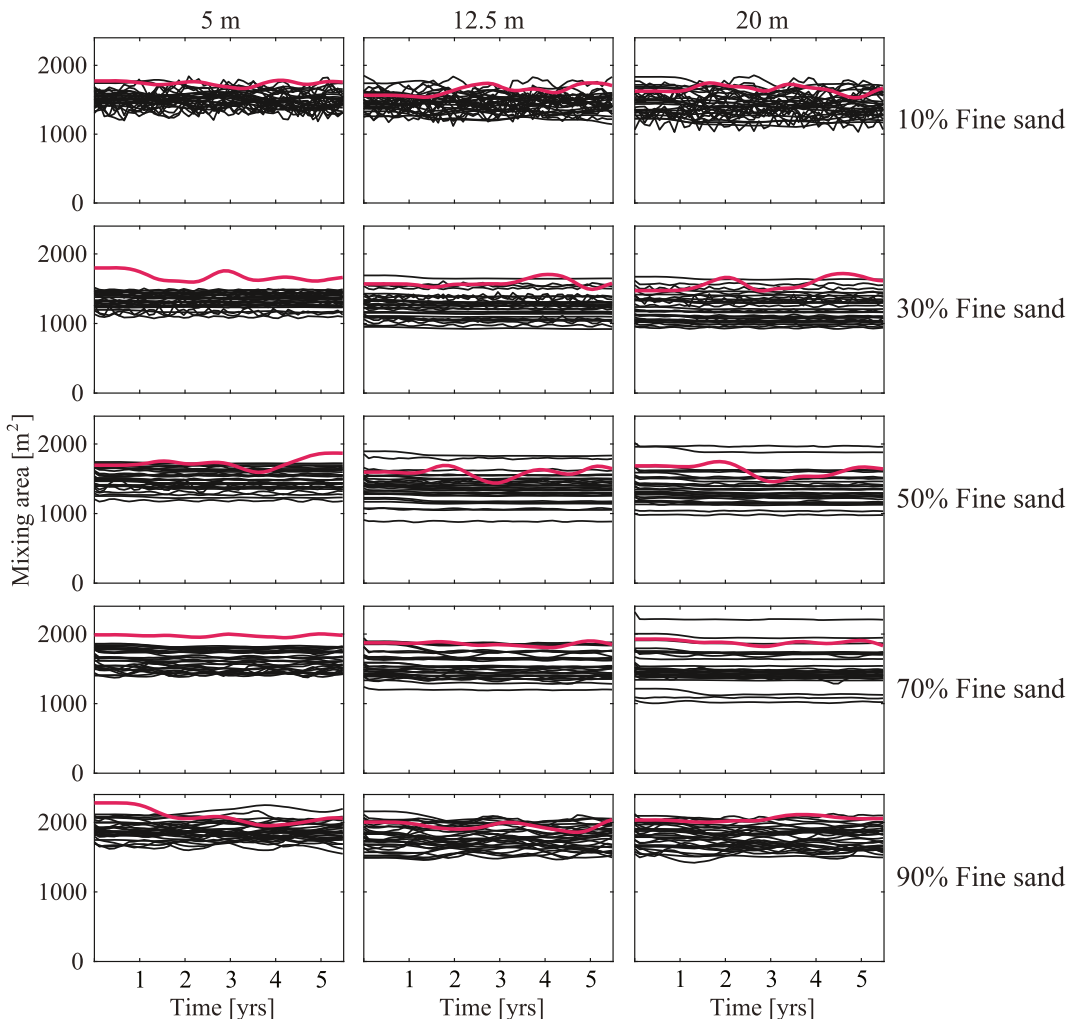


Figure 11. Intertidal mixing zone size for the heterogeneous model ensemble members (black) and hydraulically equivalent homogeneous models (red) for the three horizontal ranges (columns) and five proportions of fine sand (rows).

mixing zone is a hotspot for biogeochemical reactions involving carbon, nitrate, iron, and sulfate. For example, Kim et al. (2017) found that the highest rates of aerobic respiration and denitrification were inside the intertidal mixing zone. Further, Beck et al. (2017) demonstrated that chemical processes in a beach aquifer along the German coast were tied to the spatial distribution of fresh and saline pore water. These studies highlight the importance of accurately estimating the spatial extent and timescales of variability of the intertidal mixing zone when predicting material fluxes to the ocean. Numerical models can be used to achieve such objectives. However, most modeling studies involving tidal- or wave-influenced beach aquifers assume homogeneity. This study suggests that it is important to incorporate geologic heterogeneity into models of systems prone to unstable flow when estimating chemical fluxes to the ocean. The reason is twofold.

First, the intertidal mixing zone in the heterogeneous models was smaller than the hydraulically equivalent homogeneous models (Figure 9). As reactivity is strongly linked to mixing area, assuming homogeneity in reactive transport models of beach aquifers could overestimate the spatial extent or intensity of biogeochemical reactions, leading to simulated nutrient fluxes that underestimate real-world fluxes. Model results demonstrated that the degree of heterogeneity was the primary control on mixing area, while the connectedness of sand bodies was of secondary importance (Figure 9). Hence, geologic data consisting of the relative proportion of facies types could serve as valuable input to geostatistical and numerical models for improving chemical flux estimates in beach aquifers where unstable flow may occur.

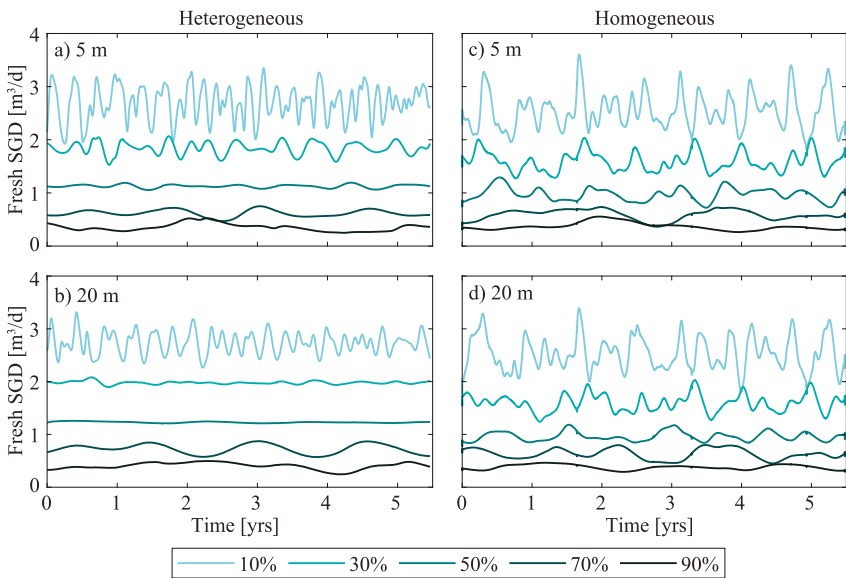


Figure 12. Tidally-averaged fresh SGD for example heterogeneous models (left panels) and hydraulically equivalent homogeneous models (right panels). The top panels show low geologic continuity (5 m horizontal variogram range) and the bottom panels show high geologic continuity (20 m horizontal variogram range). The line colors are the five fine sand proportions.

Second, salinity in the heterogeneous models was less variable over time, particularly for cases with moderate to high heterogeneity (Figures 7 and 8). Microbial communities that process nitrogen can uniquely adapt to intermediate salinity where salt concentrations are steady (Crump et al., 2004), and intermediate salinity zones in beaches can have the highest species richness (Santoro et al., 2006). Because geologic heterogeneity is ubiquitous and promotes invariant salinity, this suggests a larger fraction of beach aquifers may contain a rich community of specialized microorganisms, rather than organisms tolerant to a wide range of salinity (Santoro, 2010). However, microbial communities can also immigrate with a moving saltwater-freshwater interface (Santoro et al., 2008) and can reactivate quickly upon exposure to optimal coastal aquifer conditions (Ruiz-González et al., 2021). Thus, the implications of a more stable mixing zone on chemical processing will ultimately depend on the rate at which microbial assemblages immigrate and activate/deactivate relative to the timescales of fingering flow and corresponding shifts in reactant supply. Reactive transport models that incorporate microbial growth and decay (e.g., Xian et al., 2023) provide an avenue for investigating these coupled microbial-biogeochemical-hydrological processes.

4.3. Implications for Coastal Engineering and Management

The findings from this study have implications in coastal engineering. Beach nourishment is an engineering approach increasingly used worldwide as means for restoring the amount of sand on beaches. A principle design consideration of beach nourishment is the grain size of the nourished sediment, which should match the native beach grain size to ensure the beach maintains its characteristics important for recreation, wildlife, and storm protection. However, nourished beaches rarely re-create the sediment structure of the beach (Fegley et al., 2020) because the borrow sites are chosen according to sediment availability and economic considerations, rather than solely for grain size compatibility (Staudt et al., 2021). This creates spatial variability of beach sediment grain size (Peterson et al., 2014). Extending the results of the study herein, engineered geologic heterogeneity resulting from a mismatch of native and nourished sediment is likely to create a smaller intertidal mixing zone and less dynamic pore water salinities in systems conducive to fingering flow (Figure 9). Conversely, beaches that are

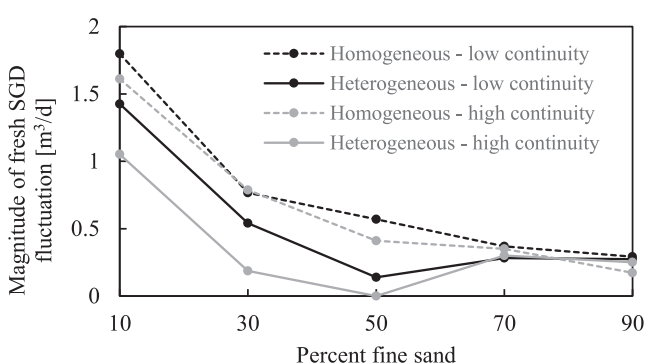


Figure 13. Magnitude of fresh SGD oscillation for the heterogeneous models (solid lines) and hydraulically equivalent homogeneous models (dashed lines). The black lines show low geology continuity (5 m horizontal range) and gray lines show high geologic continuity (20 m horizontal range).

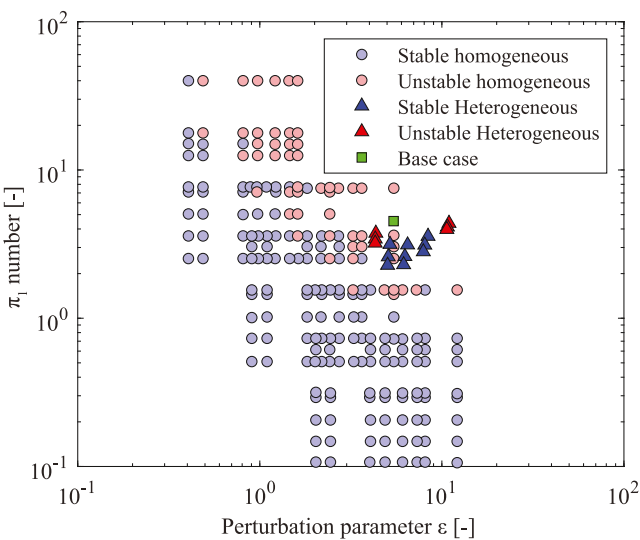


Figure 14. Stability of intertidal mixing zones in ϵ and π_1 space. The light blue and light red circles are, respectively, stable and unstable homogeneous model cases from Greskowiak (2014). The triangular symbols are ensemble results from our heterogeneous models (blue = stable, red = unstable). The green square is the homogeneous base case.

previously published homogeneous model results. Our model simulations did not consider changes in tidal amplitude over fortnightly or monthly spring-neap cycles (Abarca et al., 2013; Buquet et al., 2016; Heiss & Michael, 2014; C. Robinson, Gibbes, et al., 2007), which create temporal variations in salt mass influx rates across the upper beachface (Abarca et al., 2013). Pulses of saltwater entering the beach from spring-neap cycling could perturb the system, generating salt fingers from heightened system transience. To evaluate the effect of a sinusoidal tide, we conducted simulations with spring-neap tidal cycles. An example time series of the tidal water levels applied in the spring-neap models is shown in Figure S16 (Supporting Information S1) and details of the tidal harmonics used to generate the spring-neap tidal signal are provided in Text S1 (Supporting Information S1). Spring-neap forcing was tested for the 15 geologic scenarios (five degrees of heterogeneity and three levels of geologic continuity) shown in Figure 2. These spring-neap simulations were performed using one K realization for each scenario. Simulations for the other 29 realizations for each geologic scenario were not performed due to computational demands of the other 435 models that would be required for a full sensitivity analysis. Like models with sinusoidal tides, the simulated salinities showed that the mixing zone became more stable as the degree of heterogeneity and geologic continuity increased (Figure S17 in Supporting Information S1). These results suggest that the key findings of this study are applicable to beaches with realistic tidal forcing. We note that some fingering flow was found in models with 70% fine sand, which demonstrates more free convective motion relative to the same set of models with a sinusoidal tide (Figure S17 in Supporting Information S1). However, unstable flow was comparatively more muted in cases with 10% fine sand.

The same dispersivity values were assigned to the homogeneous and heterogeneous models. This created a lack of full equivalence in the homogeneous models because heterogeneity increases effective dispersivity. However, it was not possible to determine effective longitudinal and transverse dispersivity values for the 450 K realizations. To investigate a possible role of effective dispersivity, we varied dispersivity in the hydraulically equivalent homogeneous models and through trial and error found that a longitudinal dispersivity of 1.5 m and a transverse dispersivity of 0.15 m most closely approximated the extent of finger development in the heterogeneous models (Figure S18 in Supporting Information S1). However, as expected, there were discrepancies because the same pair of effective dispersivity values were applied in all homogeneous models, and effective dispersivity will ultimately vary with each unique bimodal K realization and resulting velocity field (Rubin, 1995). In these homogeneous models with elevated dispersivity, there was less fingering flow in the 10% and 90% proportions relative to the heterogeneous counterparts (Figure S18 in Supporting Information S1 vs. Figure 5). Conversely, density fingers were more pronounced in the 30%–70% proportions compared to the heterogeneous models. These additional

nourished with sediment of a size similar to the native beach will have a more homogeneous sediment structure, and our study suggests that this homogeneity will create a larger mixing zone due to dynamic fingering flow and downward convection of salt into the deeper aquifer. Larger intertidal mixing zones can support greater denitrification, thereby reducing high nitrate loads to the coastal ocean (Heiss et al., 2017). Thus, our study highlights a potentially new motive for matching native and nourished beach sediment. Coastal managers and engineers can weigh these new insights when selecting sediment borrow sites, especially in cases where a key objective of nourishment is optimizing beach ecosystem services. There has been an exponential growth in sand volume placed on beaches through nourishment over the last century (Elko et al., 2021). If this trend continues, the importance of sediment matching as it relates to groundwater chemical fluxes to the ocean may become even more important in the future, especially as nutrient inputs to coastal waters increase from population growth (Bricker et al., 2008).

4.4. Study Considerations

The objective of this study was to understand the role of complex geologic heterogeneity on the stability of beach saltwater-freshwater mixing zones. This was carried out with simplified numerical models that neglected several hydrologic forcings that drive flow and salt transport in intertidal sediments. The models assumed a sinusoidal tide for isolating geologic controls on salinity dynamics and to enable comparison of our heterogeneous models to

model simulations suggest that the smearing effect of heterogeneity on salt fingers can be captured with more accurate effective dispersivity coefficients in homogeneous models. While the hydraulically equivalent homogeneous models presented in Figure 6 likely underestimated dispersion, the strong control of heterogeneity on suppressing fingering flow is clear.

The models omitted seasonal changes in freshwater inflow and its effects on mixing zone stability. Under seasonal freshwater forcing, the mixing zone can undergo a dynamic transformation of stability-instability and tends to be more unstable compared to systems with fixed freshwater flux (Fang, Zheng, Guo, et al., 2022; Fang, Zheng, Wang, et al., 2022). While seasonal freshwater inflow can increase the potential for unstable flow, enhanced dispersion from complex heterogeneity would likely still counteract the tendency for fingering flow, based on the K fields considered herein. Therefore, the main finding of the present study—that heterogeneous assemblages of geologic facies promotes stable flow in beach aquifers—also likely holds for systems where freshwater inflow varies seasonally.

The simulated salinities captured only one possible K contrast for each geologic scenario. The low-K sediment class was assigned a K value of 2 m/d and the high-K sediment class was assigned a K value of 18 m/d, representing mild heterogeneity even for cases with sediments composed of half of each sediment type. To evaluate the importance of K contrast between the low- and high-K aggregates, we performed simulations with a higher K contrast. We assigned the low-K sediment a K value of 1 m/d and the high-K sediment a value of 100 m/d, resulting in a K contrast of 100, substantially higher than the K contrast of nine assigned in all other models. Similar to models with a K contrast of nine, the mixing zone was stable at higher degrees of heterogeneity (Figure S19 in Supporting Information S1). In Figure S19, the vertical protrusions of salt that resemble salt fingers in sediments with 30%–70% fine sand were at steady-state, again revealing preferential high-K flow paths extending from the sand surface to the deeper aquifer. In some model cases, multiple distinct regions of elevated salinity formed under the intertidal zone. For example, two separate regions of pore water with salinity between 25 and 35 ppt formed under the beachface in the model case with a 20 m horizontal range and 70% fine sand (Figure S19 in Supporting Information S1). Similarly, a small saltwater circulation zone formed in the very shallow subsurface of the fresh discharge zone in the case with a 5 m horizontal range and 30% fine sand (Figure S19 in Supporting Information S1). These model results show that multiple steady-state saltwater circulation zones can form in beach aquifers with geologic heterogeneity. These findings are analogous to the model results of Michael et al. (2016), who demonstrated that complex geologic heterogeneity can create separate saltwater circulation cells in continental shelf sediments.

While this study evaluated mixing processes for 15 geologic scenarios (five degrees of heterogeneity and three levels of geologic continuity), the simulated distributions of fine and medium sand bodies likely simplified real-world geologic structure in intertidal zones. Other K distributions comprising other horizontal and vertical correlation lengths, facies orientations, and sediment classes are warranted for delineating stable and unstable flow criteria in systems with geologic characteristics that differ from those considered here. The models were also based on two-dimensional permeability distributions and thus neglect alongshore preferential flow and transport paths that form in three-dimensional heterogeneous fields (Pool et al., 2015). Future studies should consider these additional geologic factors to further improve understanding of the conditions that promote or suppress free convection in intertidal mixing zones.

5. Conclusions

We performed numerical groundwater flow and salt transport simulations with binary distributions of fine and medium sand to investigate controls of geologic heterogeneity on free convection and the formation of salt fingers in tidally-influenced beaches. Pore water salinity dynamics were analyzed in heterogeneous sediments across five fine and medium sand proportions and three levels of geologic continuity. Our sensitivity analysis confirmed the hypothesis that heterogeneity inhibits salt finger formation and promotes a stable intertidal mixing zone due to enhanced dispersion. Fingering flow did not occur in models with moderate to high heterogeneity (30%–70% fine sand) yet was prevalent in homogeneous models with equivalent hydraulic properties. More connected geologic structure produced a more stable mixing zone compared to less connected geology for the same proportion of fine and medium sand, indicating that geologic continuity also controls salinity dynamics in beaches. The intertidal mixing zone was consistently smaller in heterogeneous cases than in the homogeneous counterparts owing to a reduction in the downward convection of salt.

The study findings suggest that salt fingering in beach aquifers may be less common than previously thought and provide a possible explanation for the lack of observed fingering flow in real beaches despite the growing body of field observations of salinity distributions in these systems. This highlights the importance of considering permeability heterogeneity when aiming to better understand the onset of fingering flow in the intertidal zone and subsequent timescales of fresh groundwater discharge across the aquifer-ocean interface. The controls of heterogeneity on fingering flow, as demonstrated in this study, can also inform interpretation of measured salinity distributions and dynamics, as well as spatial and temporal patterns of fresh SGD in the subtidal zone.

Future studies should consider other factors not considered here. Our models did not consider seasonal changes in freshwater inflow, beach slope, vertical correlation lengths, facies orientation, or sediment composed of three or more classes. These additional considerations could impact free convection in heterogeneous beach aquifers and should be incorporated into future studies to better understand the prevalence of fingering flow along the world coastline. Improved knowledge of the spatial and temporal variability of salinity and flow dynamics in beach aquifers can be used to more accurately quantify fluxes of terrestrially-sourced chemicals to the ocean.

Data Availability Statement

Example model input and output files for the base case are available on CUAHSI HydroShare (Heiss, 2024).

Acknowledgments

The authors thank the MIT SuperCloud and Lincoln Laboratory Supercomputing Center for providing HPC resources and assistance running model simulations. Madelaine Griesel provided valuable assistance simulating the Henry problem for validating variable-density flow in PFLOTRAN, and we thank Aarav Singh for help generating figures. We also thank Associate Editor Daniel Fernandez-Garcia and three anonymous reviewers for their constructive feedback, which improved this manuscript. This research was supported by the U.S. National Science Foundation award EAR-1933058 to JH.

References

- Abarca, E., Karam, H., Hemond, H. F., & Harvey, C. F. (2013). Transient groundwater dynamics in a coastal aquifer: The effects of tides, the lunar cycle, and the beach profile. *Water Resources Research*, 49(5), 2473–2488. <https://doi.org/10.1002/wrcr.20075>
- Águila, J. F., McDonnell, M. C., Flynn, R., Hamill, G. A., Ruffell, A., Benner, E. M., et al. (2022). Characterizing groundwater salinity patterns in a coastal sand aquifer at Magilligan, Northern Ireland, using geophysical and geotechnical methods. *Environmental Earth Sciences*, 81(8), 1–23. <https://doi.org/10.1007/s12665-022-10357-1>
- Ahrens, J., Beck, M., Marchant, H. K., Ahmerkamp, S., Schnetger, B., & Brumsack, H. (2020). Seasonality of organic matter degradation regulates nutrient and metal net fluxes in a high energy sandy beach. *Journal of Geophysical Research: Biogeosciences*, 125(2), e2019JG005399. <https://doi.org/10.1029/2019JG005399>
- Andersen, M. S., Baron, L., Gudbjerg, J., GregerSEN, J., Chapellier, D., Jakobsen, R., & Postma, D. (2007). Discharge of nitrate-containing groundwater into a coastal marine environment. *Journal of Hydrology*, 336(1–2), 98–114. <https://doi.org/10.1016/j.jhydrol.2006.12.023>
- Andersen, M. S., Nyvang, V., Jakobsen, R., Postma, D., & Andersen, J. H. (2005). Geochemical processes and solute transport at the seawater/freshwater interface of a sandy aquifer. *Geochimica et Cosmochimica Acta*, 69(16), 3979–3994. <https://doi.org/10.1016/j.gca.2005.03.017>
- Anwar, N., Robinson, C., & Barry, D. A. (2014). Influence of tides and waves on the fate of nutrients in a nearshore aquifer: Numerical simulations. *Advances in Water Resources*, 73, 203–213. <https://doi.org/10.1016/j.advwatres.2014.08.015>
- Ataie-Ashtiani, B., Volker, R. E., & Lockington, D. A. (1999). Tidal effects on sea water intrusion in unconfined aquifers. *Journal of Hydrology*, 216(1–2), 17–31. [https://doi.org/10.1016/S0022-1694\(98\)00275-3](https://doi.org/10.1016/S0022-1694(98)00275-3)
- Batzle, M., & Wang, Z. (1992). Seismic properties of pore fluids. *Geophysics*, 57(11), 1396–1408. <https://doi.org/10.1190/1.1443207>
- Beck, M., Reckhardt, A., Amelsberg, J., Bartholomä, A., Brumsack, H. J., Cypionka, H., et al. (2017). The drivers of biogeochemistry in beach ecosystems: A cross-shore transect from the dunes to the low-water line. *Marine Chemistry*, 190, 35–50. <https://doi.org/10.1016/j.marchem.2017.01.001>
- Befus, K. M., Cardenas, M. B., Erler, D. V., Santos, I. R., & Eyre, B. D. (2013). Heat transport dynamics at a sandy intertidal zone. *Water Resources Research*, 49(6), 3770–3786. <https://doi.org/10.1002/wrcr.20325>
- Beucher, H., & Renard, D. (2016). Truncated Gaussian and derived methods. *Comptes Rendus Geoscience*, 348(7), 510–519. <https://doi.org/10.1016/j.crte.2015.10.004>
- Bricker, S. B., Longstaff, B., Dennison, W., Jones, A., Boicourt, K., Wicks, C., & Woerner, J. (2008). Effects of nutrient enrichment in the nation's estuaries: A decade of change. *Harmful Algae*, 8(1), 21–32. <https://doi.org/10.1016/j.hal.2008.08.028>
- Buquet, D., Sirieix, C., Anschutz, P., Malaurent, P., Charbonnier, C., Naessens, F., et al. (2016). Shape of the shallow aquifer at the fresh water-sea water interface on a high-energy sandy beach. *Estuarine, Coastal and Shelf Science*, 179, 79–89. <https://doi.org/10.1016/j.ecss.2015.08.019>
- Burnett, W. C., Wattayakorn, G., Taniguchi, M., Dulaiova, H., Sojisuporn, P., Rungsupa, S., & Ishitobi, T. (2007). Groundwater-derived nutrient inputs to the upper Gulf of Thailand. *Continental Shelf Research*, 27(2), 176–190. <https://doi.org/10.1016/j.csr.2006.09.006>
- Chaillou, G., Couturier, M., Tommi-Morin, G., & Rao, A. M. F. (2014). Total alkalinity and dissolved inorganic carbon production in groundwaters discharging through a sandy beach. *Procedia Earth and Planetary Science*, 10(1950), 88–99. <https://doi.org/10.1016/j.proeps.2014.08.017>
- Chaillou, G., Lemay-Borduas, F., Larocque, M., Couturier, M., Biehler, A., & Tommi-Morin, G. (2018). Flow and discharge of groundwater from a snowmelt-affected sandy beach. *Journal of Hydrology*, 557, 4–15. <https://doi.org/10.1016/j.jhydrol.2017.12.010>
- Charette, M. A., & Sholkovitz, E. R. (2002). Oxidative precipitation of groundwater-derived ferrous iron in the subterranean estuary of a coastal bay. *Geophysical Research Letters*, 29(10), 851–854. <https://doi.org/10.1029/2001gl1014512>
- Chen, K., Chen, X., Song, X., Briggs, M. A., Jiang, P., Shuai, P., et al. (2022). Using ensemble data assimilation to estimate transient hydrologic exchange flow under highly dynamic flow conditions. *Water Resources Research*, 58(5), e2021WR030735. <https://doi.org/10.1029/2021WR030735>
- Cooper, H. H. (1959). A hypothesis concerning the dynamic balance of fresh water and salt water in a coastal aquifer. <https://doi.org/10.1029/JZ064i004p00461>
- Couturier, M., Tommi-Morin, G., Sirois, M., Rao, A. M. F., Nozais, C., & Chaillou, G. (2017). Nitrogen transformations along a shallow subterranean estuary. *Biogeosciences*, 14(13), 3321–3336. <https://doi.org/10.5194/bg-14-3321-2017>

- Crump, B. C., Hopkinson, C. S., Sogin, M. L., & Hobbie, J. E. (2004). Microbial biogeography along an estuarine salinity gradient: Combined influences of bacterial growth and residence time. *Applied and Environmental Microbiology*, 70(3), 1494–1505. <https://doi.org/10.1128/AEM.70.3.1494-1505.2004>
- Deutsch, C. V., & Journel, A. G. (1997). *GSLIB: Geostatistical software library and user's guide* (2nd ed.). Oxford University Press.
- Dwivedi, D., Arora, B., Steefel, C. I., Dafflon, B., & Versteeg, R. (2018). Hot spots and hot moments of nitrogen in a riparian corridor. *Water Resources Research*, 54(1), 205–222. <https://doi.org/10.1002/2017WR022346>
- Ehlert, C., Reckhardt, A., Greskowiak, J., Liguori, B. T. P., Böning, P., Paffrath, R., et al. (2016). Transformation of silicon in a sandy beach ecosystem: Insights from stable silicon isotopes from fresh and saline groundwaters. *Chemical Geology*, 440, 207–218. <https://doi.org/10.1016/j.chemgeo.2016.07.015>
- Elko, N., Briggs, T. R., Benedet, L., Robertson, Q., Thomson, G., Webb, B. M., & Garvey, K. (2021). A century of U.S. beach nourishment. *Ocean and Coastal Management*, 199, 105406. <https://doi.org/10.1016/j.ocecoaman.2020.105406>
- Evans, T. B., & Wilson, A. M. (2017). Submarine groundwater discharge and solute transport under a transgressive barrier island. *Journal of Hydrology*, 547, 97–110. <https://doi.org/10.1016/j.jhydrol.2017.01.028>
- Fang, Y., Zheng, T., Guo, B., Zhan, H., Wang, H., Zheng, X., & Walther, M. (2022). Transformation in the stability of tide-induced upper saline plume driven by transient external forcing. *Water Resources Research*, 58(6), e2021WR031331. <https://doi.org/10.1029/2021WR031331>
- Fang, Y., Zheng, T., Wang, H., Zheng, X., & Walther, M. (2022). Influence of dynamically stable-unstable flow on seawater intrusion and submarine groundwater discharge over tidal and seasonal cycles. *Journal of Geophysical Research: Oceans*, 127(4), e2021JC018209. <https://doi.org/10.1029/2021JC018209>
- Fang, Y., Zheng, T., Zheng, X., Yang, H., Wang, H., & Walther, M. (2021). Influence of tide-induced unstable flow on seawater intrusion and submarine groundwater discharge. *Water Resources Research*, 57(4), e2020WR029038. <https://doi.org/10.1029/2020WR029038>
- Fegley, S. R., Smith, J. P. S., Johnson, D., Schirmer, A., Jones-Boggs, J., Edmonds, A., & Bursey, J. (2020). Nourished, exposed beaches exhibit altered sediment structure and meiofaunal communities. *Diversity*, 12(6), 245. <https://doi.org/10.3390/d12060245>
- Freeze, R. A., & Cherry, J. A. (1979). *Groundwater*. Prentice-Hall.
- Geng, X., Boufadel, M. C., Rajaram, H., Cui, F., Lee, K., & An, C. (2020). Numerical study of solute transport in heterogeneous beach aquifers subjected to tides. *Water Resources Research*, 56(3), e2019WR026430. <https://doi.org/10.1029/2019WR026430>
- Geng, X., Heiss, J. W., Michael, H. A., & Boufadel, M. C. (2017). Subsurface flow and moisture dynamics in response to swash motions: Effects of beach hydraulic conductivity and capillarity. *Water Resources Research*, 53(12), 10317–10335. <https://doi.org/10.1002/2017WR021248>
- Geng, X., Michael, H. A., Boufadel, M. C., Molz, F. J., Gerges, F., & Lee, K. (2020). Heterogeneity affects intertidal flow topology in coastal beach aquifers. *Geophysical Research Letters*, 47(17), e2020GL089612. <https://doi.org/10.1029/2020GL089612>
- Gibbes, B., Robinson, C., Li, L., & Lockington, D. A. (2007). Measurement of hydrodynamics and pore water chemistry in intertidal groundwater systems. *Journal of Coastal Research*, 2007(50), 884–894. <https://doi.org/10.2112/jcr-si50-164.1>
- Greskowiak, J. (2014). Tide-induced salt-fingering flow during submarine groundwater discharge. *Geophysical Research Letters*, 41(18), 6413–6419. <https://doi.org/10.1002/2014GL061184>
- Grünenbaum, N., Günther, T., Greskowiak, J., Vienken, T., Müller-Petke, M., & Massmann, G. (2023). Salinity distribution in the subterranean estuary of a meso-tidal high-energy beach characterized by Electrical Resistivity Tomography and direct push technology. *Journal of Hydrology*, 617, 129074. <https://doi.org/10.1016/j.jhydrol.2023.129074>
- Heiss, J. W. (2024). Data for “Stability of saltwater-freshwater mixing zones in beach aquifers with geologic heterogeneity” [Dataset]. *HydroShare*. <http://www.hydroshare.org/resource/4a601ece58f140669b3fe548c70189e1>
- Heiss, J. W., Mase, B., & Shen, C. (2022). Effects of future increases in tidal flooding on salinity and groundwater dynamics in coastal aquifers. *Water Resources Research*, 58(12), e2022WR033195. <https://doi.org/10.1029/2022WR033195>
- Heiss, J. W., & Michael, H. A. (2014). Saltwater-freshwater mixing dynamics in a sandy beach aquifer over tidal, spring-neap, and seasonal cycles. *Water Resources Research*, 50(8), 6747–6766. <https://doi.org/10.1002/2014WR015574>
- Heiss, J. W., Michael, H. A., & Koneshloo, M. (2020). Denitrification hotspots in intertidal mixing zones linked to geologic heterogeneity. *Environmental Research Letters*, 15(8), 084015. <https://doi.org/10.1088/1748-9326/ab90a6>
- Heiss, J. W., Post, V. E. A., Laatoe, T., Russoniello, C. J., & Michael, H. A. (2017). Physical controls on biogeochemical processes in intertidal zones of beach aquifers. *Water Resources Research*, 53(11), 9225–9244. <https://doi.org/10.1002/2017WR021110>
- Heiss, J. W., Puleo, J. A., Ullman, W. J., & Michael, H. A. (2015). Coupled surface-subsurface hydrologic measurements reveal infiltration, recharge, and discharge dynamics across the swash zone of a sandy beach. *Water Resources Research*, 51(11), 8834–8853. <https://doi.org/10.1002/2015WR017395>
- Henderson, R. D., Day-Lewis, F. D., Abarca, E., Harvey, C. F., Karam, H. N., Liu, L., & Lane, J. W., Jr. (2010). Marine electrical resistivity imaging of submarine groundwater discharge: Sensitivity analysis and application in Waquoit Bay, Massachusetts, USA. *Hydrogeology Journal*, 18(1), 173–185. <https://doi.org/10.1007/s10040-009-0498-z>
- Henry, H. R. (1964). *Effect of dispersion on salt encroachment in coastal aquifers* (pp. 70–81). U.S. Geological Survey Water-Supply.
- Hwang, D.-W., Lee, Y.-W., & Kim, G. (2005). Large submarine groundwater discharge and benthic eutrophication in Bangdu Bay on volcanic Jeju Island, Korea. *Limnology & Oceanography*, 50(5), 1393–1403. <https://doi.org/10.4319/lo.2005.50.5.1393>
- Kim, K. H., Heiss, J. W., Michael, H. A., Cai, W. J., Laatoe, T., Post, V. E. A., & Ullman, W. J. (2017). Spatial patterns of groundwater biogeochemical reactivity in an intertidal beach aquifer. *Journal of Geophysical Research: Biogeosciences*, 122(10), 2548–2562. <https://doi.org/10.1002/2017JG003943>
- Kim, K. H., Heiss, J. W., Michael, H. A., Ullman, W. J., & Cai, W.-J. (2022). Seasonal and spatial production patterns of dissolved inorganic carbon and total alkalinity in a shallow beach aquifer. *Frontiers in Marine Science*, 9(6), 1–12. <https://doi.org/10.3389/fmars.2022.856281>
- Kroeger, K. D., Swarzenski, P. W., Greenwood, W. J., & Reich, C. (2007). Submarine groundwater discharge to Tampa Bay: Nutrient fluxes and biogeochemistry of the coastal aquifer. *Marine Chemistry*, 104(1–2), 85–97. <https://doi.org/10.1016/j.marchem.2006.10.012>
- Kuan, W. K., Xin, P., Jin, G., Robinson, C. E., Gibbes, B., & Li, L. (2019). Combined effect of tides and varying inland groundwater input on flow and salinity distribution in unconfined coastal aquifers. *Water Resources Research*, 55(11), 8864–8880. <https://doi.org/10.1029/2018WR024492>
- Langevin, C. D., Thorne, D. T., Jr., Dausman, A. M., Sukop, M. C., & Guo, W. (2008). SEAWAT version 4: A computer program for simulation of multi-species solute and heat transport.
- Li, X., Hu, B. X., Burnett, W. C., Santos, I. R., & Chanton, J. (2009). Submarine ground water discharge driven by tidal pumping in a heterogeneous aquifer. *Ground Water*, 47(4), 558–568. <https://doi.org/10.1111/j.1745-6584.2009.00563.x>
- Lichtner, P. C., Hammond, G. E., Lu, C., Karra, S., Bisht, G., Andre, B., et al. (2015). PFLOTRAN user manual a massively parallel reactive flow and transport model for describing surface and subsurface processes.

- Liu, Y., Jiao, J. J., Liang, W., & Luo, X. (2017). Tidal pumping-induced nutrients dynamics and biogeochemical implications in an intertidal aquifer. *Journal of Geophysical Research: Biogeosciences*, 122(12), 3322–3342. <https://doi.org/10.1002/2017JG004017>
- Mao, X., Enot, P., Barry, D. A., Li, L., Binley, A., & Jeng, D.-S. (2006). Tidal influence on behaviour of a coastal aquifer adjacent to a low-relief estuary. *Journal of Hydrology*, 327(1–2), 110–127. <https://doi.org/10.1016/j.jhydrol.2005.11.030>
- McAllister, S. M., Barnett, J. M., Heiss, J. W., Findlay, A. J., MacDonald, D. J., Dow, C. L., et al. (2015). Dynamic hydrologic and biogeochemical processes drive microbially enhanced iron and sulfur cycling within the intertidal mixing zone of a beach aquifer. *Limnology & Oceanography*, 60(1), 329–345. <https://doi.org/10.1111/lo.10029>
- Michael, H. A., Mulligan, A. E., & Harvey, C. F. (2005). Seasonal oscillations in water exchange between aquifers and the coastal ocean. *Nature*, 436(7054), 1145–1148. <https://doi.org/10.1038/nature03935>
- Michael, H. A., Post, V. E. A., Wilson, A. M., & Werner, A. D. (2017). Science, society, and the coastal groundwater squeeze. *Water Resources Research*, 53(4), 2610–2617. <https://doi.org/10.1002/2017WR020851>
- Michael, H. A., Scott, K. C., Koneshloo, M., Yu, X., Khan, M. R., & Li, K. (2016). Geologic influence on groundwater salinity drives large seawater circulation through the continental shelf. *Geophysical Research Letters*, 43(20), 10782–10791. <https://doi.org/10.1002/2016GL070863>
- Mualem, Y. (1976). A new model for predicting the hydraulic conductivity of unsaturated porous media. *Water Resources Research*, 12(3), 513–522. <https://doi.org/10.1029/WR012i003p00513>
- Nakajima, T., Sugimoto, R., Kusunoki, T., Yokoyama, K., & Taniguchi, M. (2021). Nutrient fluxes from rivers, groundwater, and the ocean into the coastal embayment along the Sanriku ria coast, Japan. *Limnology & Oceanography*, 66(7), 2728–2744. <https://doi.org/10.1002/lo.11785>
- Oostrom, M., Hayworth, J. S., Dane, J. H., & Güven, O. (1992). Behavior of dense aqueous phase leachate plumes in homogeneous porous media. *Water Resources Research*, 28(8), 2123–2134. <https://doi.org/10.1029/92WR00711>
- Peng, K., Heiss, J. W., Xie, X., Yan, L., Deng, Y., Gan, Y., et al. (2023). Groundwater discharge and saltwater-freshwater mixing in a mangrove wetland over tidal cycles: A field and modeling study. *Journal of Hydrology*, 620, 129472. <https://doi.org/10.1016/j.jhydrol.2023.129472>
- Peterson, C. H., Bishop, M. J., D'Anna, L. M., & Johnson, G. A. (2014). Multi-year persistence of beach habitat degradation from nourishment using coarse shelly sediments. *Science of the Total Environment*, 487, 481–492. <https://doi.org/10.1016/j.scitotenv.2014.04.046>
- Pool, M., Post, V. E. A., & Simmons, C. T. (2015). Effects of tidal fluctuations and spatial heterogeneity on mixing and spreading in spatially heterogeneous coastal aquifers. *Water Resources Research*, 51(3), 1570–1585. <https://doi.org/10.1002/2014WR016068>
- Reckhardt, A., Beck, M., Greskowiak, J., Schnetger, B., Böttcher, M. E., Gehre, M., & Brumsack, H.-J. (2017). Cycling of redox-sensitive elements in a sandy subterranean estuary of the southern North Sea. *Marine Chemistry*, 188, 6–17. <https://doi.org/10.1016/j.marchem.2016.11.003>
- Reckhardt, A., Beck, M., Seidel, M., Riedel, T., Wehrmann, A., Bartholomä, A., et al. (2015). Carbon, nutrient and trace metal cycling in sandy sediments: A comparison of high-energy beaches and backbarrier tidal flats. *Estuarine, Coastal and Shelf Science*, 159, 1–14. <https://doi.org/10.1016/j.ecss.2015.03.025>
- Reeves, H. W., Thibodeau, P. M., Underwood, R. G., & Gardner, L. R. (2000). Incorporation of total stress changes into the ground water model SUTRA. *Ground Water*, 38(1), 89–98. <https://doi.org/10.1111/j.1745-6584.2000.tb00205.x>
- Remy, N., Boucher, A., & Wu, J. (2009). Applied geostatistics with SGeMS: A users' guide. Retrieved from <http://sgems.sourceforge.net/>
- Richards, L. A. (1931). Capillary conduction of liquids through porous mediums. Retrieved from http://jap.aip.org/about/rights_and_permissions
- Riedel, T., Lettmann, K., Schnetger, B., Beck, M., & Brumsack, H.-J. (2011). Rates of trace metal and nutrient diagenesis in an intertidal creek bank. *Geochimica et Cosmochimica Acta*, 75(1), 134–147. <https://doi.org/10.1016/j.gca.2010.09.040>
- Robinson, C., Gibbes, B., Carey, H., & Li, L. (2007). Salt-freshwater dynamics in a subterranean estuary over a spring-neap tidal cycle. *Journal of Geophysical Research*, 112(9), C09007. <https://doi.org/10.1029/2006JC003888>
- Robinson, C., Gibbes, B., & Li, L. (2006). Driving mechanisms for groundwater flow and salt transport in a subterranean estuary. *Geophysical Research Letters*, 33(3), L03402. <https://doi.org/10.1029/2005GL025247>
- Robinson, C., Li, L., & Barry, D. A. (2007). Effect of tidal forcing on a subterranean estuary. *Advances in Water Resources*, 30(4), 851–865. <https://doi.org/10.1016/j.advwatres.2006.07.006>
- Robinson, C., Li, L., & Prommer, H. (2007). Tide-induced recirculation across the aquifer-ocean interface. *Water Resources Research*, 43(7). <https://doi.org/10.1029/2006WR005679>
- Robinson, M., Gallagher, D., & Reay, W. (1998). Field observations of tidal and seasonal variations in ground water discharge to tidal estuarine surface water. *Groundwater Monitoring & Remediation*, 18(1), 83–92. <https://doi.org/10.1111/j.1745-6592.1998.tb00605.x>
- Röper, T., Greskowiak, J., & Massmann, G. (2015). Instabilities of submarine groundwater discharge under tidal forcing. *Limnology & Oceanography*, 60(1), 22–28. <https://doi.org/10.1002/lo.10005>
- Roy, M., Martin, J. B., Cable, J. E., & Smith, C. G. (2013). Variations of iron flux and organic carbon remineralization in a subterranean estuary caused by inter-annual variations in recharge. *Geochimica et Cosmochimica Acta*, 103, 301–315. <https://doi.org/10.1016/j.gca.2012.10.055>
- Roy, M., Martin, J. B., Cherrier, J., Cable, J. E., & Smith, C. G. (2010). Influence of sea level rise on iron diagenesis in an east Florida subterranean estuary. *Geochimica et Cosmochimica Acta*, 74(19), 5560–5573. <https://doi.org/10.1016/j.gca.2010.07.007>
- Rubin, Y. (1995). Flow and transport in bimodal heterogeneous formations. *Water Resources Research*, 31(10), 2461–2468. <https://doi.org/10.1029/95WR01953>
- Ruiz-González, C., Rodellas, V., & García-Orellana, J. (2021). The microbial dimension of submarine groundwater discharge: Current challenges and future directions. *FEMS Microbiology Reviews*, 45(5), fuab010. <https://doi.org/10.1093/femsre/fuab010>
- Santoro, A. E. (2010). Microbial nitrogen cycling at the saltwater-freshwater interface. *Hydrogeology Journal*, 18(1), 187–202. <https://doi.org/10.1007/s10040-009-0526-z>
- Santoro, A. E., Boehm, A. B., & Francis, C. A. (2006). Denitrifier community composition along a nitrate and salinity gradient in a coastal aquifer. *Applied and Environmental Microbiology*, 72(3), 2102–2109. <https://doi.org/10.1128/AEM.72.3.2102-2109.2006>
- Santoro, A. E., Francis, C. A., De Sieyes, N. R., & Boehm, A. B. (2008). Shifts in the relative abundance of ammonia-oxidizing bacteria and archaea across physicochemical gradients in a subterranean estuary. *Environmental Microbiology*, 10(4), 1068–1079. <https://doi.org/10.1111/j.1462-2920.2007.01547.x>
- Santos, I. R., Chen, X., Lecher, A. L., Sawyer, A. H., Moosdorf, N., Rodellas, V., et al. (2021). Submarine groundwater discharge impacts on coastal nutrient biogeochemistry. *Nature Reviews Earth & Environment*, 2(5), 307–323. <https://doi.org/10.1038/s43017-021-00152-0>
- Schinariol, R. A., Schwartz, F. W., & Mendoza, C. A. (1994). On the generation of instabilities in variable density flow. *Water Resources Research*, 30(4), 913–927. <https://doi.org/10.1029/93WR02951>
- Schinariol, R. A., Schwartz, F. W., & Mendoza, C. A. (1997). Instabilities in variable density flows: Stability and sensitivity analyses for homogeneous and heterogeneous media. *Water Resources Research*, 33(1), 31–41. <https://doi.org/10.1029/96WR02587>

- Seidel, M., Beck, M., Greskowiak, J., Riedel, T., Waska, H., Suryaputra, I. G. N. A., et al. (2015). Benthic-pelagic coupling of nutrients and dissolved organic matter composition in an intertidal sandy beach. *Marine Chemistry*, 176, 150–163. <https://doi.org/10.1016/j.marchem.2015.08.011>
- Shen, C., Zhang, C., Kong, J., Xin, P., Lu, C., Zhao, Z., & Li, L. (2019). Solute transport influenced by unstable flow in beach aquifers. *Advances in Water Resources*, 125, 68–81. <https://doi.org/10.1016/j.advwatres.2019.01.009>
- Simmons, C. T., Fenstemaker, T. R., & Sharp, J. M. (2001). Variable-density groundwater flow and solute transport in heterogeneous porous media: Approaches, resolutions and future challenges. *Journal of Contaminant Hydrology*, 52(1–4), 245–275. [https://doi.org/10.1016/s0169-7722\(01\)00160-7](https://doi.org/10.1016/s0169-7722(01)00160-7)
- Sirois, M., Couturier, M., Barber, A., Gélinas, Y., & Chaillou, G. (2018). Interactions between iron and organic carbon in a sandy beach subterranean estuary. *Marine Chemistry*, 202, 86–96. <https://doi.org/10.1016/j.marchem.2018.02.004>
- Slomp, C. P., & Van Cappellen, P. (2004). Nutrient inputs to the coastal ocean through submarine groundwater discharge: Controls and potential impact. *Journal of Hydrology*, 295(1–4), 64–86. <https://doi.org/10.1016/j.jhydrol.2004.02.018>
- Song, X., Chen, X., Stegen, J., Hammond, G., Song, H., Dai, H., et al. (2018). Drought conditions maximize the impact of high-frequency flow variations on thermal regimes and biogeochemical function in the hyporheic zone. *Water Resources Research*, 54(10), 7361–7382. <https://doi.org/10.1029/2018WR022586>
- Sous, D., Petitjean, L., Bouchette, F., Rey, V., Meulé, S., Sabatier, F., & Martins, K. (2016). Field evidence of swash groundwater circulation in the microtidal Rousy beach, France. *Advances in Water Resources*, 97, 144–155. <https://doi.org/10.1016/j.advwatres.2016.09.009>
- Staudt, F., Gijsman, R., Ganai, C., Mielck, F., Wolbring, J., Hass, H. C., et al. (2021). The sustainability of beach nourishments: A review of nourishment and environmental monitoring practice. *Journal of Coastal Conservation*, 25(2), 34. <https://doi.org/10.1007/s11852-021-00801-y>
- Taniguchi, M., Burnett, W. C., Cable, J. E., & Turner, J. V. (2002). Investigation of submarine groundwater discharge. *Hydrological Processes*, 16(11), 2115–2129. <https://doi.org/10.1002/hyp.1145>
- Taniguchi, M., Dulai, H., Burnett, K. M., Santos, I. R., Sugimoto, R., Stieglitz, T., et al. (2019). Submarine groundwater discharge: Updates on its measurement techniques, geophysical drivers, magnitudes, and effects. *Frontiers in Environmental Science*, 7, 141. <https://doi.org/10.3389/fenvs.2019.00141>
- Thorn, P., & Urich, D. W. (2013). Preliminary observation of complex salt-fresh water mixing in a beach aquifer. *Ground Water*, 51(1), 145–150. <https://doi.org/10.1111/j.1745-6584.2012.00947.x>
- Trezzi, G., Garcia-Orellana, J., Rodellas, V., Santos-Echeandia, J., Tovar-Sánchez, A., García-Solsona, E., & Masqué, P. (2016). Submarine groundwater discharge: A significant source of dissolved trace metals to the North Western Mediterranean Sea. *Marine Chemistry*, 186, 90–100. <https://doi.org/10.1016/j.marchem.2016.08.004>
- Urich, D. W., & McKenna, T. E. (2004). Tidal effects on ground water discharge through a sandy marine beach. *Ground Water*, 42(7), 971–982. <https://doi.org/10.1111/j.1745-6584.2004.tb02636.x>
- Vandenbohede, A., & Lebbe, L. (2006). Occurrence of salt water above fresh water in dynamic equilibrium in a coastal groundwater flow system near De Panne, Belgium. *Hydrogeology Journal*, 14(4), 462–472. <https://doi.org/10.1007/s10040-005-0446-5>
- Van Genuchten, M. T. (1980). A closed-form equation for predicting the hydraulic conductivity of unsaturated soils. *Soil Science Society of America Journal*, 44(5), 892–898. <https://doi.org/10.2136/sssaj1980.03615995004400050002x>
- Voss, C. I., & Provost, A. M. (2010). SUTRA a model for saturated-unsaturated, variable-density ground-water flow with solute or energy transport (SUTRA Version 2.2) Reston, Virginia 2010 i. Retrieved from <http://water.usgs.gov/nrp/gwsoftware>
- Wallace, C. D., Sawyer, A. H., Barnes, R. T., Soltanian, M. R., Gabor, R. S., Wilkins, M. J., & Moore, M. T. (2020). A model analysis of the tidal engine that drives nitrogen cycling in coastal riparian aquifers. *Water Resources Research*, 56(4), e2019WR025662. <https://doi.org/10.1029/2019wr025662>
- Waska, H., Greskowiak, J., Ahrens, J., Beck, M., Ahmerkamp, S., Böning, P., et al. (2019). Spatial and temporal patterns of pore water chemistry in the inter-tidal zone of a high energy beach. *Frontiers in Marine Science*, 6. <https://doi.org/10.3389/fmars.2019.00154>
- Wilson, A. M., & Gardner, L. R. (2006). Tidally driven groundwater flow and solute exchange in a marsh: Numerical simulations. *Water Resources Research*, 42(1), W01405. <https://doi.org/10.1029/2005WR004302>
- Xian, Y., Wen, Z., Jin, M., Liang, X., & Jakada, H. (2023). Groundwater-borne nitrate removal within heterogeneous sediments under interactions between hydraulics, nutrients, and biofilms. *Journal of Hydrology*, 616, 128777. <https://doi.org/10.1016/j.jhydrol.2022.128777>
- Xin, P., Jin, G., Li, L., & Barry, D. A. (2009). Effects of crab burrows on pore water flows in salt marshes. *Advances in Water Resources*, 32(3), 439–449. <https://doi.org/10.1016/j.advwatres.2008.12.008>
- Xin, P., Robinson, C., Li, L., Barry, D. A., & Bakhtyar, R. (2010). Effects of wave forcing on a subterranean estuary. *Water Resources Research*, 46(12), W12505. <https://doi.org/10.1029/2010WR009632>
- Xing, C., Zhang, Y., Guo, X., & Sun, J. (2023). Time series investigation of electrical resistivity tomography reveals the key drivers of tide and storm on groundwater discharge. *Estuarine, Coastal and Shelf Science*, 282, 108225. <https://doi.org/10.1016/j.ecss.2023.108225>
- Zamora, P. B., Cardenas, M. B., & Cook, P. L. M. (2021). Groundwater–surface water interactions in a river estuary and the importance of geomorphology: Insights from hydraulic, thermal and geophysical observations. *Hydrological Processes*, 35(10). <https://doi.org/10.1002/hyp.14372>
- Zhang, J., Lu, C., Shen, C., Zhang, C., Kong, J., & Li, L. (2021). Effects of a low-permeability layer on unstable flow pattern and land-sourced solute transport in coastal aquifers. *Journal of Hydrology*, 598, 126397. <https://doi.org/10.1016/j.jhydrol.2021.126397>
- Zhang, Y., Li, L., Erler, D. V., Santos, I., & Lockington, D. (2017). Effects of beach slope breaks on nearshore groundwater dynamics. *Hydrological Processes*, 31(14), 2530–2540. <https://doi.org/10.1002/hyp.11196>
- Zhang, Y., Xing, C., Guo, X., Zheng, T., Zhang, K., Xiao, X., et al. (2023). Temporal and spatial distribution patterns of upper saline plumes and seawater-groundwater exchange under tidal effect. *Journal of Hydrology*, 625, 130042. <https://doi.org/10.1016/j.jhydrol.2023.130042>